

An Offprint from

Lectures in
**APPLIED
MATHEMATICS**



American Mathematical Society
Providence, Rhode Island

A dynamical systems analysis of kinematics in the time-periodic wake of a circular cylinder

K. SHARIFF, T.H. PULLIAM & J.M. OTTINO

Abstract. Stable and unstable manifolds of dynamical systems theory are used to study the motion and deformation of fluid elements for flow past a circular cylinder in the regime of time-periodic vortex shedding; Reynolds numbers of 100 and 180 are considered. The existence of manifolds is guaranteed only for hyperbolic periodic points but in the present case the entire body surface consists of non-hyperbolic periodic points. Therefore conditions are derived for the existence of a manifold at the body surface. These conditions imply that while a separation point in instantaneous streamline portraits may wander in time, particle trajectories separate from the wall at single points. A hyperbolic periodic point is found in the wake; the intersection of its manifolds with the manifolds of surface points provides information about fluid engulfment into- and shedding from the wake cavity. For $Re = 180$ the fraction of the fluid in the cavity shed every period is larger leading to a smaller residence time. Calculation of the manifolds with adaptive resolution allows one to delineate the topology of the intersection pattern and how it changes with Reynolds number.

Computed manifolds agree well with streaklines for a range of injection locations near the body and give a good indication of regions which have maximum extension or compression. For example, line elements that stretch the most are initially close and normal to the stable manifold and end-up near and parallel to the unstable manifold.

1. Introduction. This work has two chief objectives: (i) To employ tools from dynamical systems theory, namely, the stable and unstable manifolds, to study the processes of fluid engulfment and shedding in the unsteady wake of a circular cylinder. (ii) To test the usefulness of the unstable manifold as a numerical flow visualization aid for unsteady two-dimensional bluff body flows. The word "manifold" should evoke in the mind of the

1991 *Mathematics Subject Classification*: Primary 34C35, 76D25; Secondary 76D15.

A detailed version of this paper will be submitted for publication elsewhere.

©1991 American Mathematical Society
0075-8485/91 \$1.00 + \$.25 per page

reader only the simple ideas of curve or surface and none of the forbidding notions of abstract spaces. For steady flow, the stable or unstable manifolds are simply what a fluid mechanician refers to as a separating streamline, dividing streamline or separatrix. The background for the generalization of these concepts to time-periodic flow will be disclosed in §2.

With respect to the first objective, very little is known about transport in the near wakes of bluff bodies. Those who have been interested in the operation of flame-holders and electrostatic precipitators (see, for example, Winterfeld [28] and Vincent [27]) often speak of an ill-defined region which traps fluid behind the body, loosely identifying it with the recirculation bubble of the time-averaged flow. Perry, Chong and Lim [16] described the entrainment process in terms of 'alleyway' regions in instantaneous streamline portraits. By simultaneous observation of streaklines and instantaneous streamlines at different phases during the shedding cycle, they were able to make the following, in our view remarkable, deduction: " 'bodies' of fluid form a queue and are successively stacked up one behind the other and then move in jumps towards the solid body, awaiting their turn to be 'squeezed' out of the cavity and carried away by a Kelvin-Helmholtz-like roll-up." It seemed to us that with the help of dynamical systems theory, one could sharpen the description of this process by defining more precisely what is meant by "wake cavity", "bodies of fluid" and by quantifying rates of transport.

With respect to the second objective, calculations undertaken for the periodic leapfrogging of two vortex rings (Shariff *et al.* [20], [21]) illustrated the striking property of the unstable manifold to reveal even very fine scale features of flow visualization using a patch of smoke. We inquire as to whether the same property may apply to the streak method of visualization for bluff body flows. That it may is suggested by a thought provoking sketch in Perry, Chong and Lim [16] (their Figure 8) of the threading of a streakline. To someone a little familiar with dynamical systems, its pattern of multiple folding and layering looks very much like a portrait of a manifold.

The paper is organized as follows. The next section (§2) provides the necessary dynamical systems background, with the goal of defining the stable and unstable manifolds. The section concludes with some new results concerning the issuance of manifolds from solid walls. Section 3 discusses the numerical procedures used for obtaining the velocity field, for tracking particles and computing manifolds. The presentation of results in §4 is divided into sub-sections. It begins in the first sub-section with a conventional Eulerian view of the flow by presenting instantaneous streamline portraits in order to orient the reader to the type of unsteadiness present. The second sub-section presents manifolds for Reynolds numbers of 100 and 180 and compares fluid transport characteristics and the topology of the manifolds for the two cases. The next sub-section discusses the relationship between manifolds, streaklines and the underlying vorticity field. The fourth sub-section is devoted to a study of the deformation of infinitesimal line elements and serves to rationalize the relationships observed between streaklines and the unstable manifold. We are also motivated in

this work by
grangian ar
of Kurosaka
temperature
may have an
with recom

2. Dyna
define the st
of the text b
and slope of
The equa
two dimensi

(1)

The solution
albeit at dif
this, introdu

(2)

If the velocit
 ϕ be modulo

We shall w
column vecto
and f_i , respe

The numb
a map. For
(Poincaré) m
to ϕ_0 as the
we may cons
like the pairin
map. In eithe
for the desire

(3)

where x and
level. For th
which displac
map and its r

For both th
local properti

this work by the possibility of explaining interesting physical effects by Lagrangian arguments. To this end, the last sub-section verifies the suggestion of Kurosaka *et al.* [12], that the phenomenon of reversal of time-averaged temperature gradient downstream of a circular cylinder (Minchin [15]), may have an explanation in terms of particle trajectories. The paper closes with recommendations for further work.

2. Dynamical systems terminology. The goal of this section is to define the stable and unstable manifolds, drawing upon the first few pages of the text by Guckenheimer and Holmes [8], and then to discuss the points and slope of manifold emanation from a solid no-slip surface.

The equations of motion of a material point (henceforth "particle") in two dimensional unsteady flow are

$$(1) \quad \begin{aligned} \dot{x} &= u(x, y, t), \\ \dot{y} &= v(x, y, t). \end{aligned}$$

The solution curves of (1) in the xy plane may cross for different particles, albeit at different t . This fact impairs geometric thinking. To overcome this, introduce time as an extra dimension:

$$(2) \quad \begin{aligned} \dot{x} &= u(x, y, \phi), \\ \dot{y} &= v(x, y, \phi), \\ \dot{\phi} &= 1. \end{aligned}$$

If the velocity is time-periodic, with period 2π say, then it is enough that ϕ be modulo 2π to ensure non-crossing trajectories in $xy\phi$ space.

We shall write systems such as (2) simply as $\dot{\mathbf{x}} = \mathbf{f}(\mathbf{x})$ where \mathbf{x} and \mathbf{f} are column vectors with n elements; we shall denote their i th elements as x_i and f_i , respectively.

The number of dimensions of the problem is reduced to two by defining a map. For example for a time-periodic velocity we may consider the (Poincaré) map of particles in one period $\phi_o \rightarrow \phi_o + 2\pi$. We shall refer to ϕ_o as the base phase of the Poincaré map. For a non-periodic velocity we may consider how particles are mapped during some interesting event like the pairing of two vortices in a mixing layer; we shall call this an event map. In either case integrating the dynamical system, usually numerically, for the desired time interval and then iterating the map we get

$$(3) \quad \mathbf{x}^{i+1} = \mathbf{g}(\mathbf{x}^i),$$

where \mathbf{x} and \mathbf{g} have $n-1$ elements and the superscript denotes the iteration level. For the event map, iteration gives a chain of particles, each one of which displaces its iterate during the event. The usefulness of the event map and its manifolds remains untested.

For both the continuous system and map one may begin by studying the local properties of the system. This is possible in the vicinity of its fixed

points, \bar{x} , defined so that

$$(4) \quad \begin{aligned} f(\bar{x}) &= 0 \quad (\text{continuous system}), \\ g(\bar{x}) &= \bar{x} \quad (\text{map}). \end{aligned}$$

A fixed point of the Poincaré map corresponds to a particle with a periodic trajectory. Note that the continuous system (2) has no fixed points but it may have a periodic trajectory. The local behavior near the fixed point is investigated by studying the linearized systems

$$(5) \quad \begin{aligned} \dot{\xi} &= A\xi \quad (\text{continuous system}), \\ \xi^{i+1} &= B\xi^i \quad (\text{map}), \\ \xi &\equiv x - \bar{x}, \end{aligned}$$

where A and B are the Jacobian matrices of $f(x)$ and $g(x)$, respectively. A fixed point of a continuous system is called hyperbolic if A contains no eigenvalues with zero real part; a fixed point of a map is hyperbolic if B contains no eigenvalues with unit modulus. For a continuous system, the spaces spanned by those generalized eigenvectors of the Jacobian matrix that are associated with the positive and negative eigenvalues, respectively, are called the unstable and stable eigenspaces. For a map, the unstable and stable eigenspaces are the spaces spanned by the generalized eigenvectors of B whose eigenvalues have modulus > 1 and < 1 , respectively.

It is important to realize that the solution curves of the linearized system may not be geometrically related to those of the fully nonlinear system in the vicinity of the fixed point, except for a hyperbolic fixed point. The Hartman-Grobman theorem assures one that for a hyperbolic fixed point the two can be deformed to each other in a continuous, invertible and one-to-one fashion. For solid surfaces on which the no-slip and impermeability

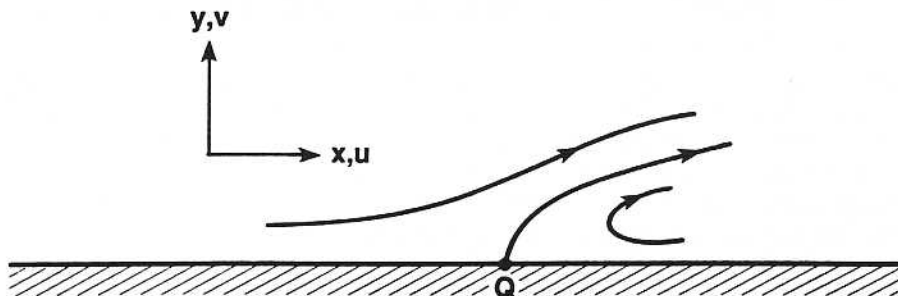


FIGURE 1. Sketch of streamline pattern for steady separated flow over a flat wall.

conditions are specified, the entire surface consists of non-hyperbolic fixed points, and there may be no connection between the linearized and local flow. For example, consider steady separated compressible flow over a no-slip wall; Figure 1 sketches some streamlines. The equation of mass conservation, $(\rho u)_x + (\rho v)_y = 0$, where ρ is the fluid density, allows one



FIGURE 2. about a no-s

to define a s

(6)

whose level
commas in s
expanding ψ
to bicubic te
only if $(\sigma)_w$
at the wall i

(7)

Note that th
of (7) are ill
nonlinear sy
far, the dens
the density f
conservation
on the sides
the density
streamlines.
non-zero the
wall and we
the linearize
separation p

We shall s
maps into its
started on th
line is an inv
Any set of p
times and su
chosen to be

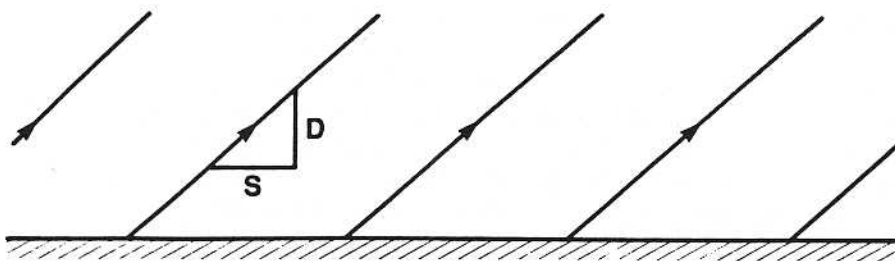


FIGURE 2. Streamline pattern for steady compressible flow linearized about a no-slip wall.

to define a streamfunction, ψ , such that

$$(6) \quad \begin{aligned} \rho u &= \psi_{,y}, \\ \rho v &= -\psi_{,x}, \end{aligned}$$

whose level curves are tangent to the velocity. Here and subsequently, commas in subscripts denote partial differentiation, e.g., $\psi_{,y} = \partial\psi/\partial y$. By expanding ψ in a Taylor series about a point on the wall (denoted by w) up to bicubic terms it is seen that the separating streamline emanates from w only if $(\sigma)_w = 0$, where $\sigma \equiv \psi_{,yy}$. The slope of the separating streamline at the wall is $-3(\sigma_{,x}/\sigma_{,y})_w$. The flow linearized about w is

$$(7) \quad \begin{pmatrix} \dot{\xi}_x \\ \dot{\xi}_y \end{pmatrix} = \begin{pmatrix} 0 & S \\ 0 & D \end{pmatrix} \begin{pmatrix} \xi_x \\ \xi_y \end{pmatrix},$$

$S \equiv (u_{,y})_w$, the shear at the wall,
 $D \equiv (v_{,y})_w$, the dilatation at the wall.

Note that the Jacobian matrix has a zero eigenvalue. The solution curves of (7) are illustrated in Figure 2; they are unrelated to those of the full nonlinear system, thus illustrating the Hartman-Grobman theorem. So far, the density in (6) has been some arbitrary function. To determine the density for the linearized flow, consider in Figure 2 the principle of conservation of mass for an area bounded on the bottom by the wall and on the sides by streamlines. We see that Figure 2 does not satisfy it unless the density is zero or the dilatation D at the wall is zero to make the streamlines of the linearized flow parallel to the wall. If the density is non-zero then the equation of mass conservation implies that $D = 0$ at the wall and we must admit the latter case. In this case, the streamlines of the linearized and actual flow become geometrically related except at the separation point Q .

We shall sometimes use the term *invariant set*. It refers to a set which maps into itself under the action of the dynamical system, i.e., a particle started on the set remains on the set forever. For steady flow, each streamline is an invariant set. Consider a Poincaré map for time-periodic flow. Any set of points S_0 iterated forward and backward an infinite number of times and superimposed, provides an invariant set for the map. If S_0 is chosen to be a curve whose endpoints are the forward or backward maps

of each other then the invariant set is a connected set. A streakline in a time-periodic flow is the forward half of an invariant set of this kind. For this case, S_0 is the streakline formed after the injection device has been on for one period. In the next period, S_0 is mapped to the curve S_1 and S_0 is recovered by the newly injected particles and so on. Hence in order to numerically calculate a streakline for a time-periodic flow at a given phase without continually injecting particles, one would simply generate S_0 by injecting particles for one period and then iterate it to obtain S_1, S_2, \dots , superimposing them on the page.

Finally, we are in a position to define the stable and unstable manifolds of a fixed point of a map or continuous system—they are merely connected invariant sets passing through the fixed point. Alternatively, we begin by defining them locally in some neighborhood B of the fixed point. The local stable (unstable) manifold is the set of all points in B which tend to the fixed point as $t \rightarrow +\infty (-\infty)$. For a map, the iteration index i plays the role of t . The global stable (unstable) manifolds are simply defined by letting the local manifolds flow backward (forward) under the action of the continuous system or map. For example, the separating streamline in Figure 1 is the only unstable manifold in the flow. Note that while every wall point is a fixed point, only one of them, namely, Q has a manifold emanating from it. This is a feature of non-hyperbolic fixed points. On the other hand, stable and unstable manifolds are guaranteed to exist for every hyperbolic fixed point and to be tangent to the stable and unstable eigenspaces of the fixed point. For closed steady separation bubbles, the separating streamline may connect to a another fixed point, say P . In this case, the separating streamline is also the stable manifold of P . This coincidence is not robust and in general, for a time periodic perturbation, two such manifolds of the Poincaré map are *split*.

Consider time-period two-dimensional fluid flow. As the base phase ϕ_0 of the Poincaré map varies, the changing manifold (an unstable one, say) of a fixed point of the map can be thought of as the changing cross-section of a surface in $xy\phi$ space. This surface is the unstable manifold of a periodic trajectory in $xy\phi$ space. The reader now knows that not only fixed points of the continuous system but also periodic trajectories may have manifolds. All the particle trajectories lying on this surface tend to the periodic one as $t \rightarrow -\infty$. It should therefore be clear that as ϕ_0 varies, the changing manifold of the Poincaré map evolves as a material curve. Like a streakline or other invariant set, it is one of the select material curves whose shape evolves in a periodic manner.

Manifold emanation point and angle for time-periodic flow over a curved wall. The existence of a manifold at a non-hyperbolic periodic point is not guaranteed. This sub-section generalizes to the time-periodic case, the result for steady flow that a manifold emanates from the point of zero shear stress. The slope of the manifold is also given.

Consider a curved wall and a curvilinear coordinate system (ξ, η) in which the wall coincides with the curve $\eta = 0$. We shall require that the coordi-

nates attain
next a Poin
denote par
ticle displa
placed at th
A manifold
slope if and
that if η_0/ξ
which may

We first c
origin. A T

(8)

(9)

In the above
 u_ξ and u_η
 η -lines resp
the geometr

(10)

The Taylor
unity at the
the conditio
 $u_{\eta,\eta} = 0$.

With the
to yield to c

(11)

Here and su

(12)

Substituting
particle in th

(13)

nates attain unit metrics at the wall; this can always be arranged. Consider next a Poincaré map from $t = 0$ to $t = T$, the period of the flow. Let ξ_o, η_o denote particle position at $t = 0$ and let $\Delta\xi(T)$ and $\Delta\eta(T)$ represent particle displacements in one period. For convenience, the origin $\xi = \eta = 0$ is placed at the candidate point on the wall from which a manifold emanates. A manifold for the Poincaré map emanates from the origin with non-zero slope if and only if in the limit as $\xi_o, \eta_o \rightarrow 0$ there exists a slope $\alpha \neq 0$ such that if $\eta_o/\xi_o = \alpha$ then $\Delta\eta(T)/\Delta\xi(T) = \alpha$. We do not consider manifolds which may be tangent to the wall.

We first calculate the displacements $\Delta\xi(T), \Delta\eta(T)$ for particles near the origin. A Taylor expansion reveals that

$$(8) \quad \frac{d\xi}{dt} = \frac{u_\xi}{h_\xi} = u_{\xi,\eta}(t)\eta + \frac{1}{2}[u_{\xi,\eta\eta}(t) + \lambda u_{\xi,\eta}(t)]\eta^2 + u_{\xi,\xi\eta}(t)\xi\eta + \mathcal{O}(\epsilon^3),$$

$$(9) \quad \frac{d\eta}{dt} = \frac{u_\eta}{h_\eta} = \frac{1}{2}u_{\eta,\eta\eta}(t)\eta^2 + \mathcal{O}(\epsilon^3).$$

In the above equations all partial derivatives are evaluated at the origin, u_ξ and u_η are the velocity components along the tangents of ξ -lines and η -lines respectively, h_ξ and h_η are the metrics along these lines, and λ is the geometric quantity,

$$(10) \quad \lambda \equiv \left[\frac{\partial}{\partial\eta} \left(\frac{1}{h_\xi} \right) \right]_{\xi=0, \eta=0}.$$

The Taylor expansions (8) and (9) make use of the fact that metrics are unity at the wall and that regardless of the nature of the coordinate system, the condition of incompressibility when evaluated at the wall implies that $u_{\eta,\eta} = 0$.

With the initial condition $\eta(0) = \eta_o = \mathcal{O}(\epsilon)$, Equation (9) is integrated to yield to consistent order

$$(11) \quad \Delta\eta(t) \equiv \eta(t) - \eta_o = \frac{1}{2}\eta_o^2 \hat{u}_{\eta,\eta\eta}(t) + \mathcal{O}(\epsilon^3).$$

Here and subsequently, hats will denote a time integral, e.g.,

$$(12) \quad \hat{u}_{\eta,\eta\eta}(t) \equiv \int_0^t u_{\eta,\eta\eta}(\phi) d\phi.$$

Substituting Equation (11) into Equation (8) gives for the motion of the particle in the ξ direction:

$$(13) \quad \frac{d\xi}{dt} = f_1(t) + \xi f_2(t) + \mathcal{O}(\epsilon^3),$$

where

$$(14) \quad \begin{aligned} f_1(t) &\equiv u_{\xi,\eta}(t)\eta_o \left(1 + \frac{1}{2}\eta_o \hat{u}_{\eta,\eta\eta}(t)\right) + \frac{1}{2}(u_{\xi,\eta\eta}(t) + \lambda u_{\xi,\eta}(t))\eta_o^2, \\ f_2(t) &\equiv u_{\xi,\eta\xi}(t)\eta_o. \end{aligned}$$

Since to leading order,

$$(15) \quad \Delta\xi(T) = \hat{u}_{\xi,\eta}(T)\eta_o + \mathcal{O}(\epsilon^2),$$

the displacement vector $(\Delta\xi(T), \Delta\eta(T))$ becomes increasingly parallel to the wall as the wall is approached unless

$$(16) \quad \hat{u}_{\xi,\eta}(T) = 0.$$

This is a necessary condition for the manifold to emanate from the origin with a finite slope ($\alpha \neq 0$). One can derive the wall shearing stress, τ (the traction vector projected on to the wall tangent), and observe that it is equal to a non-zero geometric factor times $u_{\xi,\eta}$. Therefore the condition (16) is equivalent to the vanishing of the integral of τ over one period.

To obtain the value of the slope $\alpha \equiv \lim_{\xi_o, \eta_o \rightarrow 0} \Delta\eta(T)/\Delta\xi(T)$ we need the next term in the solution of (13). The homogeneous part has the solution $Ce^{\int f_2(t) dt}$ while the form $F(t)e^{\int f_2(t) dt}$ may be assumed for a particular solution yielding

$$(17) \quad \begin{aligned} \Delta\xi(T) &\equiv \xi(T) - \xi_o \\ &= \xi_o \eta_o \hat{u}_{\xi,\eta\xi}(T) + \frac{1}{2}\eta_o^2 \hat{u}_{\xi,\eta\eta} \\ &\quad + \eta_o^2 \int_0^T u_{\xi,\eta}(\phi) \left(\frac{1}{2}\hat{u}_{\eta,\eta\eta}(\phi) - \hat{u}_{\xi,\eta\xi}(\phi) \right) d\phi. \end{aligned}$$

Using (11) and (17) and putting $\alpha = \eta_o/\xi_o$ we obtain

$$(18) \quad \alpha = \frac{\frac{1}{2}\hat{u}_{\eta,\eta\eta}(T) - \hat{u}_{\xi,\eta\xi}(T)}{\frac{1}{2}\hat{u}_{\xi,\eta\eta}(T) + \int_0^T u_{\xi,\eta}(\phi) \left(\frac{1}{2}\hat{u}_{\eta,\eta\eta}(\phi) - \hat{u}_{\xi,\eta\xi}(\phi) \right) d\phi}.$$

That the numerator of (18) be non-zero provides, together with (16), necessary and sufficient conditions for manifold emanation from the origin with finite slope. The fact that the required conditions involve integrals of periodic functions over a period means that the manifold emanation point is independent of the base phase of the Poincaré map. This was expected beforehand because the manifold evolves as a material curve with changing base phase and the velocity at the wall tends smoothly to zero (Dwight Barkley, Private communication). The condition that the numerator in (18) be non-zero means that the term in parenthesis in the integrand is non-periodic and therefore that α is always dependent on the base phase of the Poincaré map. This dependence is periodic as it should be.

If we ask the question: which particle trajectories trace their way back to the surface of the body, the answer for steady flow would be: those

trajectories
fined to be
the unstab
cross-section
Only the t
body. They
points whe
there is on
introduced
with a thic
method (T
from the w
time-averag

If the coo
ways be arr
respect to t
ibility impl

(19)

For steady
at the mani

(20)

a result obt
streamline.

3. Num
scribe an ex
developed to
Units are
ity are unity
and cylinder

Procedure
using the co
present stud
of the Reyn
The agreeme
Navier-Stok
fourth-order
advancement
factorization
the reflection
mesh with 1
The first gri
 $r = 24$. The

trajectories lying on the dividing streamline. The point of separation is defined to be where those trajectories emanate from. For time-periodic flow, the unstable manifolds of the Poincaré map for different base phases are cross-sections of an unstable manifold of the continuous dynamical system. Only the trajectories lying on this surface can trace their way back to the body. They do so to a single point, namely, where $\hat{u}_{\xi,\eta}(T) = 0$. Thus while points where instantaneous streamlines leave the body may wander in time, there is only one separation point for particle trajectories. Marker is often introduced near the surface of a body either by pre-painting the surface with a thick coat of dye (Gerrard [7]) or by the electrolytic precipitation method (Taneda [23]). The point about which tracer is observed to erupt from the wall should therefore be fixed and should reveal the point of zero time-averaged shear stress.

If the coordinate system becomes orthogonal at the wall (which can always be arranged), then α directly provides the slope of the manifold with respect to the wall. For the case of a flat wall, the equation of incompressibility implies that $u_{x,yx} = -u_{y,yy}$ so that (18) becomes

$$(19) \quad \alpha = \frac{-3\hat{u}_{x,yx}(T)}{\hat{u}_{x,yy} - 3 \int_0^T u_{x,y} \hat{u}_{x,yx}(\phi) d\phi}.$$

For steady flow over a flat wall, the value of T is immaterial, $u_{x,y}$ is zero at the manifold emanation point and Equation (19) reduces to

$$(20) \quad \alpha = -3 \frac{u_{x,yx}}{u_{x,yy}},$$

a result obtained in Lighthill ([13], p. 65) for the slope of the dividing streamline.

3. Numerical procedures. In this section we shall first briefly describe an existing code used to obtain the velocity field and then the code developed to study the motion of particles.

Units are chosen so that the radius of the cylinder and free-stream velocity are unity. The Reynolds number, Re , is based on free-stream velocity and cylinder diameter, D .

Procedure for calculating the velocity field. The velocity field is obtained using the code ARC2D of Pulliam and Steger [17]. It was validated for the present study by comparing the Strouhal number at four different values of the Reynolds number against the experimental data of Williamson [25]. The agreement is very good; see Figure 3. The code solves the compressible Navier-Stokes equations in general curvilinear coordinates using centered fourth-order space differences. The Mach number is set to 0.1 here. Time advancement is performed with the implicit Euler scheme and approximate factorization. Characteristic boundary conditions, designed to minimize the reflection of sound waves, are imposed at the outer boundary. A polar mesh with 169×65 points in the azimuthal and radial directions is used. The first grid circle adjacent to the surface is at $r = 1.04$ and the last at $r = 24$. The adequacy of the resolution was judged by using 249×131 points

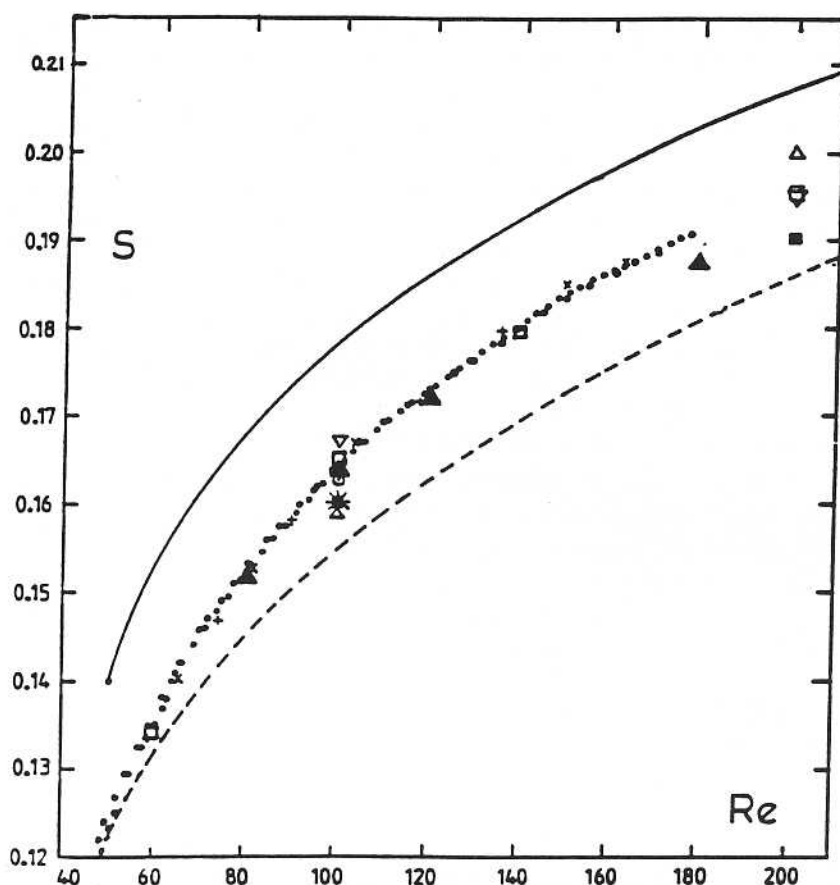


FIGURE 3. Strouhal number vs. Reynolds number compared with experiments and other computations. Small symbols: experimental data of Williamson [25]; filled triangles: present results; other symbols, solid and dashed curves: other computations. *Courtesy of Prof. C.H.K. Williamson.* For a detailed caption see Figure 7 of Williamson [25] in these proceedings.

with increased clustering near the cylinder surface (the first grid circle was at $r = 1.002$). The velocity signal at $x = y = 2$ was compared at a 151 time points in one period. The amplitude increased from .0817 to .0824 and the mean decreased from 1.234 to 1.232. The calculation of Karniadakis and Triantafyllou (Figure 9 in [11]) has a comparable amplitude of .0820 but a larger mean of 1.288.

A small amount of artificial dissipation is added to eliminate pressure oscillations at a wavelength equal to twice the mesh spacing. The calculation was started with an asymmetric initial condition and allowed to converge to a limit cycle, whereupon the period T was determined by minimizing the rms error of the x -velocity between times t and $t + T$, added to the same quantity for the y -velocity. This measure of the aperiodicity was .0008 at $Re = 80$ and .003 at $Re = 180$. Next, 600 time steps per period were executed and every fourth velocity frame was stored for the particle tracking. In order to permit future comparison with experiment or other calculations, it is important to state that the phase reference was chosen

to be the x -
in this pap
 $\Delta t = .23T$

Procedur
particle m
curvilinear

(i) Bicub
points to a
of the meri
context of l
small scales
have been
routine is v
periodic or

(ii) Parti
by unity fr
line. The o
each partic
equations o

(21)

where tildes
a grid. En
at the grid
has entries
grid-point o

(iii) Time
Since it eva
($t + 1/2\Delta t$)

(iv) Parti
stable mani

(c) Assess a
run forward

(v) Mater
refined. Th
of particles
the present
particles co
interpolation
greatly amp
(vi) Cont
along with
particles int
between the

to be the x-velocity signal at $x = y = 2$. All the Poincaré maps considered in this paper have a base phase such that this signal attains a minimum at $\Delta t = .23T$ after the base phase.

Procedure for tracking particles. A tool has been developed to study particle motions in unsteady two-dimensional velocity fields computed in curvilinear coordinates. Its main features are described below:

(i) Bicubic splines are used to interpolate the velocity field from grid points to a particle. This choice was made on the basis of an extensive study of the merits of various interpolation schemes by Yeung and Pope [30] in the context of homogeneous turbulence. While there is little energy content at small scales in the present work and bilinear interpolation would probably have been adequate, splines allow for more future flexibility. The spline routine is vectorized along one coordinate direction and has the choice of periodic or non-periodic end conditions.

(ii) Particles are tracked in grid coordinates ξ and η which increment by unity from one grid point to the next along the appropriate coordinate line. The obvious advantage is that the integer part of the coordinates for each particle provides the indices for the spline coefficient look-up. The equations of motion for a particle are

$$(21) \quad \begin{aligned} \frac{d\xi}{dt} &= \tilde{u} \left(\frac{\partial \xi}{\partial x} \right) + \tilde{v} \left(\frac{\partial \xi}{\partial y} \right), \\ \frac{d\eta}{dt} &= \tilde{u} \left(\frac{\partial \eta}{\partial x} \right) + \tilde{v} \left(\frac{\partial \eta}{\partial y} \right), \end{aligned}$$

where tildes denote the operation of spline interpolation of data stored on a grid. Entries of the coordinate Jacobian such as $\partial \xi / \partial x$ are evaluated at the grid points at program start-up from the inverse Jacobian (which has entries like $\partial x / \partial \xi$). The latter is evaluated by spline differentiation of grid-point coordinates.

(iii) Time stepping is performed with a fourth-order Runge-Kutta scheme. Since it evaluates the right hand side of Equation (21) also at the half-step $(t + 1/2\Delta t)$, with a 151 frames stored, we have 75 steps per period.

(iv) Particles may be tracked backward in time in order to (a) Obtain the stable manifolds (b) Determine the origin of interesting fluid regions and (c) Assess accuracy of time integration from the extent to which particles run forward and then backward recover the initial condition.

(v) Material curves which have lost resolution due to stretching may be refined. This is accomplished by returning to the instant at which a group of particles was injected, interpolating new particles, and tracking them to the present instant. This was considered preferable to interpolating new particles continually during the time integration. In the latter scheme, interpolation errors normal to the stretching direction would translate to greatly amplified errors in the initial configuration.

(vi) Contours of Eulerian quantities may be simultaneously presented along with particle configurations. This permits one to inject a group of particles into an interesting region of the flow or to study the relationship between the Eulerian and Lagrangian structure of the flow.

(vii) In addition to the positional degrees of freedom, deformation degrees of freedom may be evolved. An infinitesimal material line element with components l_i is tilted and stretched by the velocity field according to

$$(22) \quad \frac{Dl_i}{Dt} = \frac{\partial u_i}{\partial x_j} l_j.$$

We do not wish to track line elements with specific initial orientations; rather we wish to allow arbitrary initial orientation. For this we consider the so-called deformation gradient matrix F such that

$$(23) \quad l_i(t) = F_{ij}(t) l_j(0).$$

The four elements of F are evolved according to

$$(24) \quad \frac{DF_{im}}{Dt} = \frac{\partial u_i}{\partial x_j} F_{jm}, \quad F_{im}(0) = \delta_{im}.$$

We conclude this section by describing the calculation of manifolds. Of the several particle configurations which may be injected into the flow, is a straight line segment whose second endpoint is the map of the first during a specific duration of the flow. By iterating the map with the segment as initial condition, and superimposing the iterates on the plot, one generates an invariant set. If the first endpoint of the segment is on an unstable (stable) eigenspace very close to a hyperbolic fixed point of the map, the procedure generates a very close approximation to the unstable (stable) manifold for time running forward (backward).

It was found that a hyperbolic fixed point of the Poincaré map exists in the wake. It corresponds to a particle which has a periodic pathline. The fixed point is located by starting with a rectangle R , applying the Poincaré map T forward in time to obtain $T(R)$ and then backward in time to obtain $T^{-1}(R)$. If the map has a fixed point, it must lie in the intersection of $T(R)$ and $T^{-1}(R)$, typically a much smaller region than the original rectangle. The intersection is covered with another rectangle and the process is repeated. Eventually the mapping becomes linear and is a contraction normal to the unstable eigenspace and the inverse map is a contraction normal to the stable eigenspace. Applying to each of the two directions, the fact that every contraction mapping has a fixed point, guarantees the existence of a fixed point in the intersection. In all the cases we have considered, the amount of stretching is so large that the eigenspaces are obtained to a good approximation visually from the long sides of the stretched rectangle. If this is not the case the eigenvectors of the deformation gradient matrix for the periodic particle can be used.

The conditions for manifold emanation from a wall discussed in §2 were obtained after the calculations had been performed and were suggested by them. In order to numerically determine manifold emanation points we located, as a first step, the regions from which a band of particles near the surface erupted into the outer flow. Next, in the vicinity of these regions, a lattice of particles was iterated forward a few periods, successive iterates

FIGURE 4.
emanation p

being joined
segments ar
provides inv
visually det
manifold em
cell of $\theta = 0$
due to sym

The Navie
tracking pro
particle tra
6000) while
to an IRIS 4

4. Result

Instantan
terns for *Re*
patterns hav
tailed discus
al.(Figure 2
more than c
tex. In the
as it travels
in Figure 5b
thought tha
especially si
remained un
short-lived s
it causes the
(e) in Perry

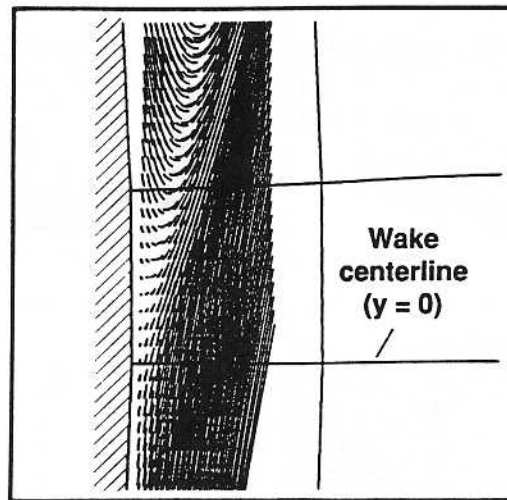


FIGURE 4. Illustration of the procedure used to locate the stable manifold emanation point at the rear surface of the cylinder.

being joined by straight line segments. To the extent that straight line segments are mapped to straight line segments near a wall, this procedure provides invariant sets from which the manifold emanation points can be visually determined. Figure 4 shows such invariant sets near the stable manifold emanation point. The manifold emanation point is within a grid cell of $\theta = 0$, a location where the time-integrated shear stress must vanish due to symmetry.

The Navier-Stokes solver (ARC2D) as well as two versions of the particle tracking program are available from the authors. The first version of the particle tracking program runs standalone on an IBM workstation (RS 6000) while the second version runs on a CRAY which issues graphics calls to an IRIS 4D-25 workstation.

4. Results.

Instantaneous streamlines. Figure 5 shows instantaneous streamline patterns for $Re = 180$ during roughly half a period of vortex shedding. Such patterns have been discussed in Perry *et al.*[16] and so do not merit detailed discussion here. Only some differences with a sketch by Perry *et al.*(Figure 2 in [16]) are worth drawing attention to. The sketch depicts more than one detached closed bubble of recirculation for each shed vortex. In the present case there is at most one bubble and it is evanescent as it travels downstream—for example, it is on the verge of disappearing in Figure 5b; this difference has also been noted by Eaton [6]. It was first thought that the disappearance may be promoted by numerical dissipation, especially since the grid becomes coarse downstream, however, the pattern remained unchanged when resolution was doubled. In Figure 5b a small short-lived secondary bubble is seen. It is not present at $Re = 100$; here it causes the size of the main bubble to rapidly increase. Sketches (d) and (e) in Perry *et al.*[16] show a discontinuous transition between having an

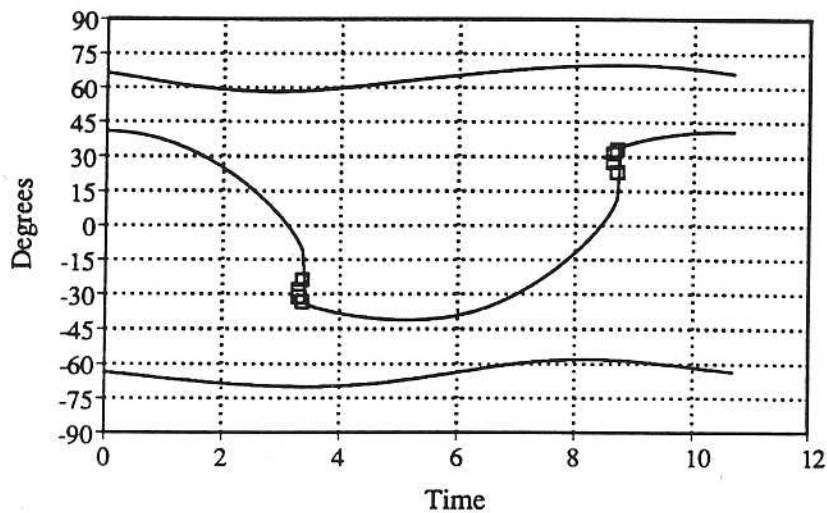


FIGURE 6. Angular position of points of zero shearing stress on the wall ($Re = 180$), measured clockwise from the leeward centerline. The open squares represent the momentary appearance of a secondary separation bubble.

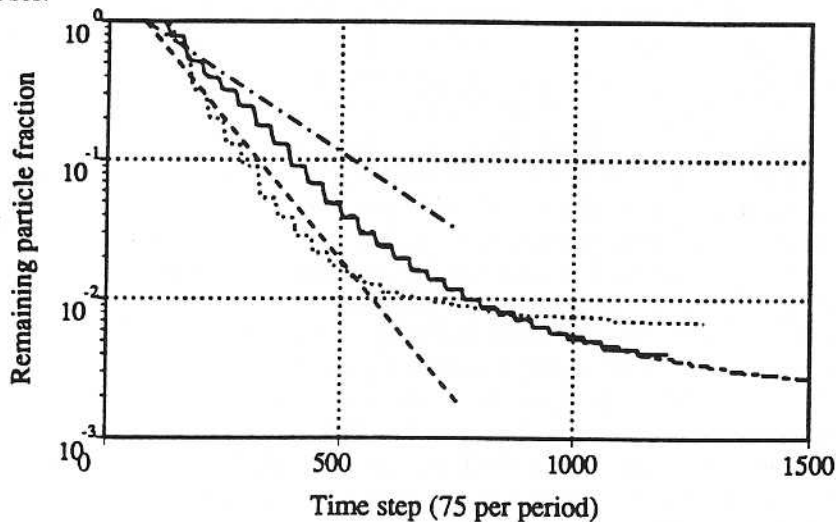


FIGURE 7. Fraction of particles remaining in the computational domain as a function of time step. —, $Re = 100$, 10^4 particles initially; ---, $Re = 100$, 10^5 particles initially; —·—, $Re = 100$, from the model equation (25); ·····, $Re = 180$, 10^4 particles initially; ----, $Re = 180$, from the model equation (25).

al.[19], discusses how they provide information about how the near wake engulfs fluid and sheds fluid into the wake, and discusses the topology of the intersection pattern of stable and unstable manifolds.

The residence time, t_R , of fluid particles behind a bluff body is a design parameter for flameholders and electrostatic precipitators [28], [27].

It is operationally defined by filling the near wake with smoke and then interrupting the supply of smoke. Thereafter, the decay of concentration in a small measurement volume is obtained by absorption techniques. Following some delay time, the decay of concentration is exponential with some superimposed fluctuations; however, Winterfeld [28] has noted deviations from exponential decay. A non-dimensional characteristic decay time $H \equiv Ut_R/D$ is defined.

For the computations, 10^4 particles were initialized behind the cylinder and allowed to escape; Figure 7 is a log-linear plot of the fraction of particles remaining in the computational domain. Since particles which leave the near wake are washed downstream, the number of particles in the near wake is obtained by translating the curves to the left. The behavior is not exponential nor was a power law observed on log-log axes. To ensure that this was not due to sampling error, the initial number of particles was increased to 10^5 for $Re = 100$ (chain-dashed line); no change is observed. The rate of decay for $Re = 180$ (dotted line) is initially larger than for $Re = 100$, but subsequently it is smaller. A value for H was obtained by determining the time interval required for the number of particles to diminish by a factor of e^{-1} , starting after $3\frac{1}{3}$ periods to avoid the initial transients. For $Re = 100$ and 180 , respectively, $H = 11.2$ and 5.6 . On the other hand, for flat plates normal to the stream, MacLennan and Vincent [14] found experimentally that H is a strongly decreasing function of Re up to about $Re = 5000$ and then asymptotes to a constant value of about $H = 5$. At the lowest Reynolds number they considered ($Re = 1000$), $H = 25$. These values happen to be comparable to the simulations at much lower Reynolds numbers, presumably because cylinders have smaller regions of trapping behind them than flat plates.

Manifolds allow one to define precisely what experimentalists have called the "trapping region behind the body" and they contain information about the decay curves discussed in the previous paragraphs. Figure 8a shows for $Re = 100$ a close-up near the body of the unstable manifold (of the Poincaré map) of the upper emanation point U and the upper half of the stable manifold of the point W in the wake having a periodic trajectory. Figure 8b is the corresponding plot for the lower side of the wake and is included only to illustrate the fact that the manifolds of the upper and lower halves of the wake hardly intermingle; the hook labelled h is the first hint of cross-talk between the two halves.

The manifolds are shown in a distorted but topologically correct sketch in Figure 9. Only the unstable manifold of U is illustrated up to the detail computed; the other manifolds are abbreviated since they have the same winding pattern. Since a particle started on one of the manifolds must end up somewhere else on it after one period, intersection points must map to intersection points. In particular in the present case, point O maps to B and A to C . Therefore the fluid in the shaded lobe labelled D_1 maps to D_2 , etc. The ends of these lobes lie inside the cores of the upper street of vortices. For points p such as O , A , B and C , the unstable manifold from U to p and the stable manifold from W to p intersect only at p . Such points are called primary intersection points [18]; the term 'lobe', which we employed earlier without definition, refers to regions bounded by segments of the unstable and stable manifolds between two such adjacent points.



FIGURE 8. (a) Close-up of the upper half of the wake showing the unstable manifold of U and the upper half of the stable manifold of W . (b) Close-up of the lower half of the wake showing the manifolds of the lower half of the wake and a hook labelled h .

The fluid in the shaded lobe D_1 maps to D_2 , etc. The ends of these lobes lie inside the cores of the upper street of vortices. For points p such as O , A , B and C , the unstable manifold from U to p and the stable manifold from W to p intersect only at p . Such points are called primary intersection points [18]; the term 'lobe', which we employed earlier without definition, refers to regions bounded by segments of the unstable and stable manifolds between two such adjacent points.

In winding

stable manifold

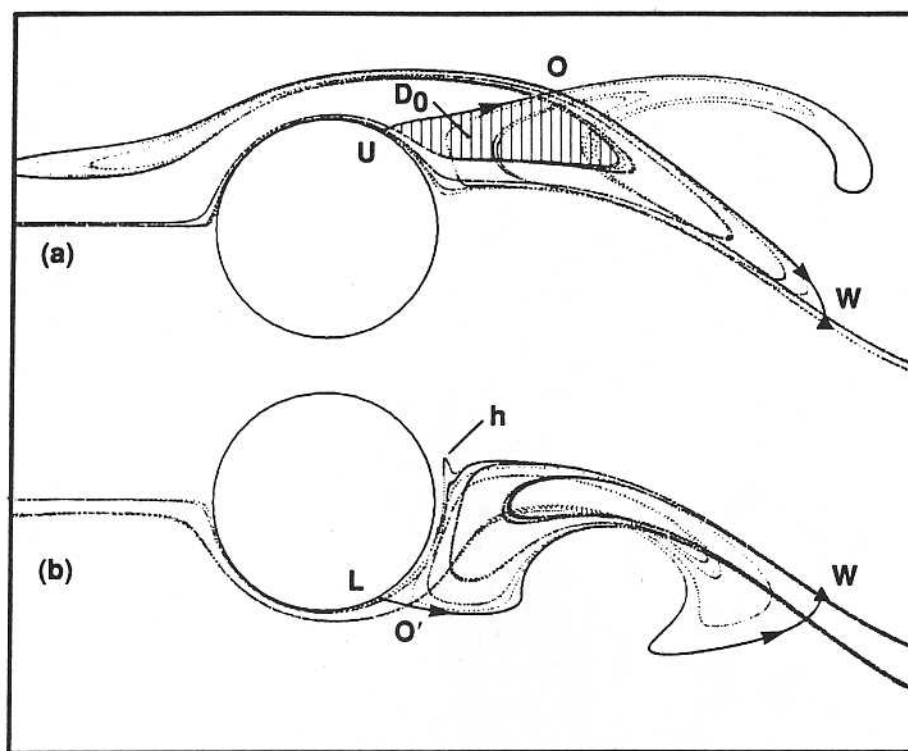


FIGURE 8. Close-up near the cylinder of four manifolds for $Re = 100$. The solid triangle indicates the periodic point W which returns to its original position after one period. (a) Two manifolds of the upper wake: unstable manifold of U and upper stable manifold of W . The shaded region of fluid escapes the upper half of the wake cavity after one period. (b) Two manifolds of the lower wake: unstable manifold of L and lower stable manifold of W .

The fluid D_1 was mapped from D_0 . The lobe D_0 is also shown shaded in the computed manifolds, Figure 8. The mass of each lobe must be the same and it will be denoted by m_L . Let us define the wake cavity as the region $UOWO'LU$ which is alternately bounded by segments of the unstable and stable manifolds. Lobe D_0 is the only fluid region (together with its counterpart on the lower side) which escapes the wake cavity after one period. It will be called the detrained lobe. All other fluid remains in the cavity. The fresh fluid that takes its place comes from the dot-filled region E_{-1} and it gets mapped to lobe E_0 . This lobe will be called the entrained lobe, and its iterates will be denoted E_1, E_2, \dots . We shall adopt the convention that the last in the sequence D -lobes and the first in the sequence of E -lobes contained completely in any defined cavity are to be numbered zero. The intersection of E_0 with D_0 is that subset of fresh fluid which will spend only one period in the cavity before escaping. This subset will escape the cavity and end-up inside D_1 as $E_1 \cap D_1$.

In winding about each other, the unstable manifold of U and the upper stable manifold of W follow a simple rule: every E_i lobe must have exactly

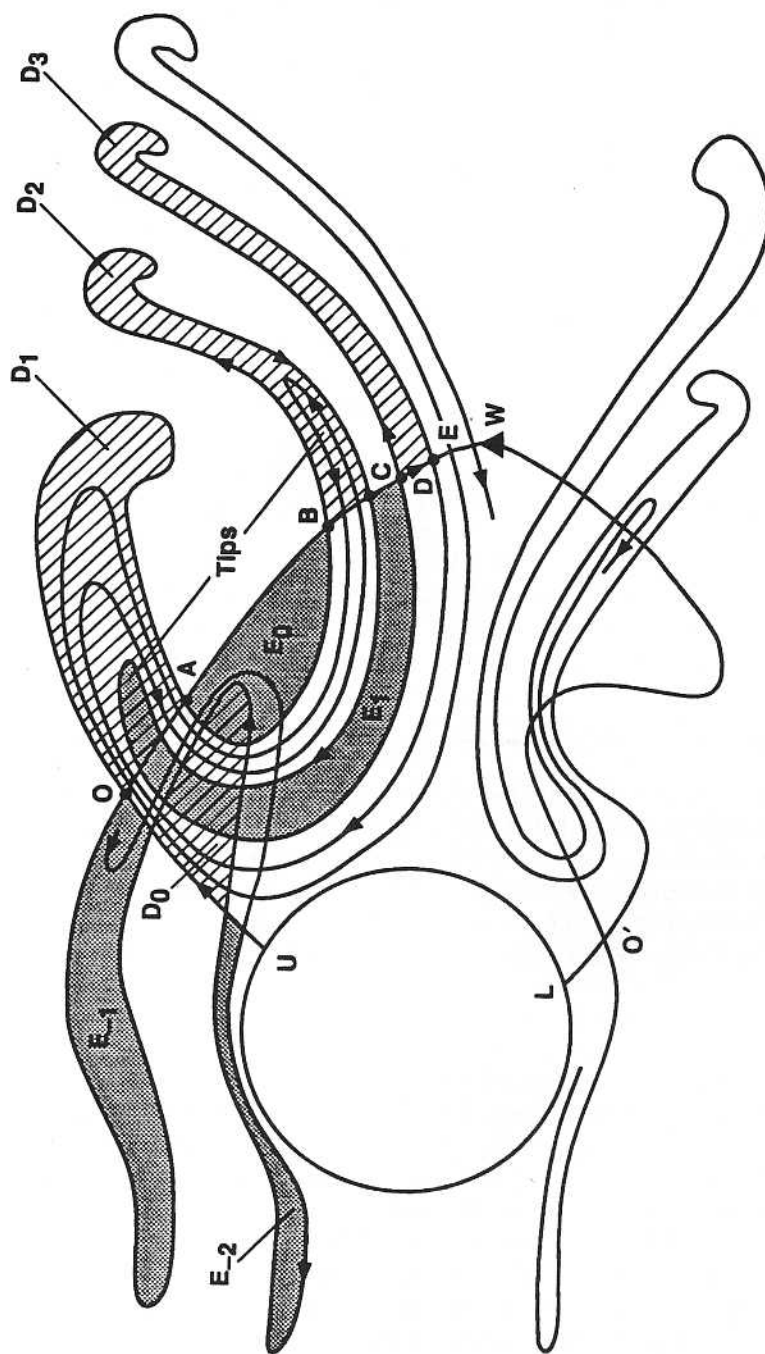


FIGURE 9. 'Threading diagram' of the four manifolds plotted in Figure 8 for $Re = 100$. The regions labelled D_i are successive iterates of the fluid, D_0 , detrained from the upper half of the wake cavity. The regions labelled E_i are iterates of the fluid E_0 entrained into the cavity.

one tip and section of a than the us rule, notice manifold wi out to form one step in back and fo sketch in Pe each vortex at $Re = 80$, is unchange does show t the sketch. of cartoons of Easton's It is possible Reynolds nu each E_i lobe

The defin One may ad example star we could ha However this for the wind unstable man the unstable at the point prescription definiteness,

Consider a that at perio ambient fluid cavity after many applic cavity is stir lobe is the s r_n must dec

(25)

in each peri For a compl the manifold et al.[19] sh between the To obtain a how much n

(26)

one tip and the tip must lie in D_i . By tip, Rom-Kedar [18] means an intersection of an E and a D lobe which has only two intersection points (rather than the usual four) of the stable and unstable manifolds. In following this rule, notice in Figure 9, how after having formed lobe D_3 at point E , the manifold winds in to form a tip in the *previous* lobe, D_2 , and then winds out to form the next lobe, D_4 . The process then repeats. In order to make one step in the process, the unstable manifold has to travel several times back and forth between the cylinder and vortices. On the other hand, the sketch in Perry *et al.* shows a streakline travelling once from the cylinder to each vortex and back. The sketch in Perry *et al.* is based on observations at $Re = 80$, hence it was verified that the computed pattern at $Re = 80$ is unchanged. The two-color photograph in Perry *et al.* (Figure 7 in [16]) does show that the streak "line" has additional structure not depicted in the sketch. The computed pattern is called Smale's horseshoe in the book of cartoons by Abraham and Shaw (pp. 95-96) [1] and is a special case of Easton's type- l trellises, as described by Rom-Kedar [18], with $l = 1$. It is possible that type- l trellises with $l > 1$ would be observed at lower Reynolds number. They are similar to the type-1 trellis but with a "delay": each E_i lobe must form a tip in D_{i-l+1} .

The definition of the wake cavity as $UOWO'LU$ is not a unique one. One may add a portion and remove another in our current definition. For example starting at the point U and travelling along the unstable manifold we could have switched to the other manifold at point B instead of at O . However this cavity has the same mass and results in the same prescription for the winding pattern. This is true for all other cavities for which the unstable manifold leaves the cavity at the switch point. If on the other hand the unstable manifold enters the cavity at the switch point (for example at the point A), then the area of such cavities is greater by m_L and the prescription of the winding pattern needs a shift in the lobe index. For definiteness, we shall always employ the former type of cavity.

Consider again the numerical experiment for particle depletion. Suppose that at period zero the cavity is filled with red fluid surrounded by clear ambient fluid. We wish to know how much red fluid, r_n , remains in the cavity after n periods. An often used engineering model of transport in many applications is that of the well-stirred reactor. If we assume that the cavity is stirred to the extent that the number of particles in the detrained lobe is the same as in any other region of the same mass in the cavity, then r_n must decrease by a factor

$$(25) \quad f = 1 - 2m_L/m_C,$$

in each period. This behavior is plotted as the straight lines in Figure 7. For a complete description one needs to consider the detailed structure of the manifolds. In particular, for the oscillating vortex pair, Rom-Kedar *et al.* [19] showed that r_n can be determined from the areas of intersection between the iterates E_i of the entrained lobe and the first shed lobe, D_1 . To obtain a similar result for the present case, first note that if we know how much *net* clear fluid, c_j enters the cavity during period j , then

$$(26) \quad r_n = m_C - \sum_{j=1}^n c_j,$$

where m_C denotes the mass of the cavity. Next, determine c_j . The amount of clear fluid which *enters* during period j is simply $2m_L$. The amount of clear fluid which *leaves* during period j consists of four types of fluid, namely, clear fluid of the upper/lower stream being discharged into the upper/lower street of vortices. Furthermore, each type of fluid is composed of clear fluid with a range of ages, a . For example consider fluid of the upper stream detrained into the upper row of vortices. Fluid that entered during period $j - a$ which leaves in period j is $E_a \cap D_1$ ($j - 1 \leq a \leq 1$). Summing over the ages and the four types gives

$$(27) \quad c_j = 2m_L - \sum_{a=1}^{j-1} \mu(E_a \cap D_1) + \mu(E'_a \cap D'_1) + \mu(E_a \cap D'_1) + \mu(E'_a \cap D'_1),$$

where μ denotes the mass of its argument and a prime denotes the corresponding region in the lower half of the cavity. The symmetries of the problem imply that the first two terms in (27) must be equal to each other as must the last two. With Equations (26) and (27), decay curves can be obtained by simply tracking particles in E_o . Ultimately, however, one would like to have a model which requires as little information about the map as possible.

Figures 10–11 repeat Figures 8–9 for $Re = 180$. There are three main differences with $Re = 100$.

(i) In Figure 10 the shaded area represents, once again, the fluid shed

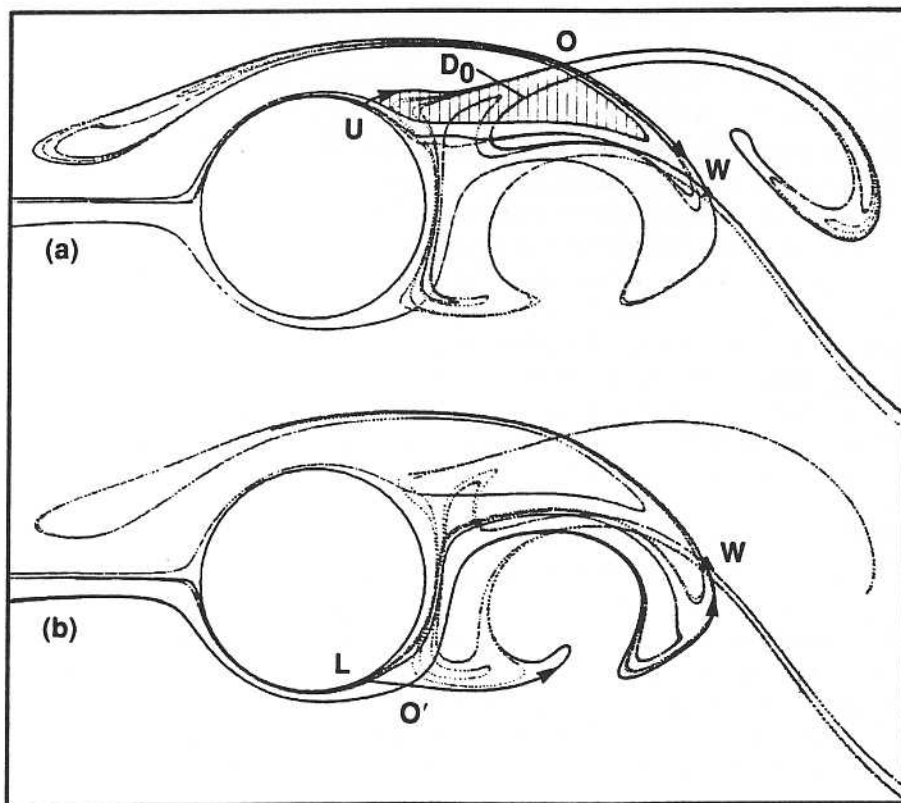


FIGURE 10. Close-up near the cylinder of four manifolds for $Re = 180$. See the caption of Figure 8 for additional details.



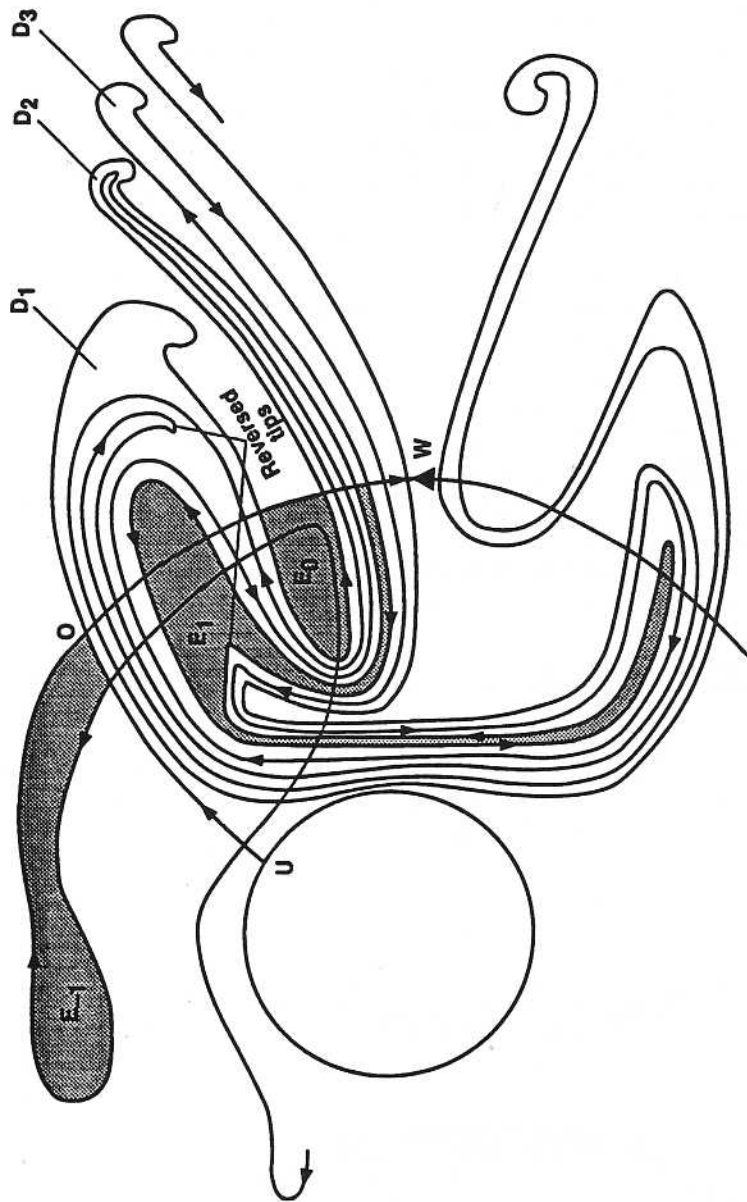


FIGURE 11. Sketch of the winding pattern of the four manifolds plotted in Figure 10 ($Re = 180$).

from the upper half cavity after one period. While its area is nearly identical to that for $Re = 100$, the area of the cavity is smaller. Hence, a larger fraction (.50 versus .32) of the cavity is shed in each period, leading to a faster initial decay rate of r_n . Experimentalists have noted a correlation between the size of recirculation zone of the time averaged flow and such quantities as the residence time (e.g. Humphries and Vincent [10]) and flame blow-off velocity (Zukoski and Marble [33]). Hence, it is of interest to note that the reduced cavity size is also manifested as a reduced size of the recirculation zone for the time averaged flow (see Figure 12), however, the recirculation zones are larger than the cavities by 22% and 24% for $Re = 100$ and $Re = 180$, respectively.

(ii) As shown in Figure 11, the winding pattern with respect to the other, of the unstable manifold of U and the upper stable manifold of W has changed. Each lobe E_i must have, not only a tip in D_i as before, but also a six point intersections in D_{i-1} , forming what is labelled as a "reversed tip." In following this rule notice how, after forming lobe D_3 , the unstable manifold travels back and forth between the cavity and vortices in order to form a tip in the previous lobe, D_2 , then winds out completely. So far, this is identical to $Re = 100$. However, then the manifold winds in again

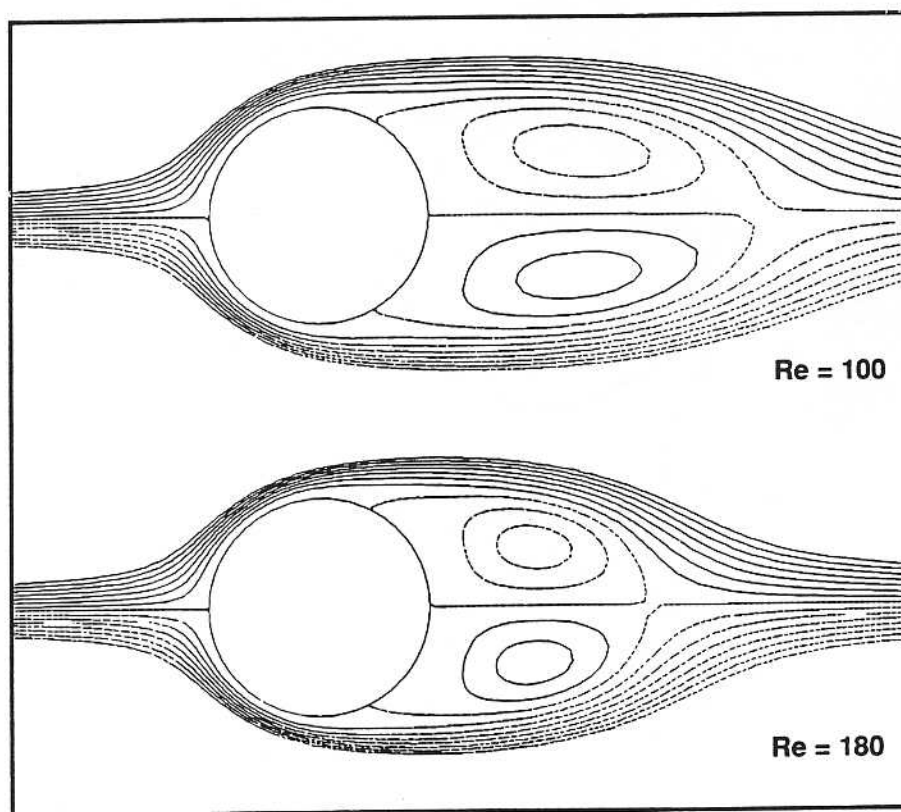


FIGURE 12. Streamfunction, averaged over one period, illustrating the reduced size of the recirculation zone for $Re = 180$. Fifteen contour levels are shown in the range $[-.2, .2]$.

to form a
to form the
does not fa
[18].

(iii) The
the wake f
manifold o
implies tra
fluid which
opposite si
upper stre
one period
rate of tra
can be qua
point M in
point W .
boundary
is shown u



FIGURE 13. Streamfunction, averaged over one period, illustrating the reduced size of the recirculation zone for $Re = 180$. Fifteen contour levels are shown in the range $[-.2, .2]$.

to form a reversed tip in the *next to previous* lobe, D_1 , before winding out to form the next lobe, D_4 ; the process then repeats. This winding pattern does not fall into the extended class of trellises considered by Rom-Kedar [18].

(iii) There is more intertwining of the manifolds from the two sides of the wake for $Re = 180$ than for $Re = 100$. For example, the unstable manifold of U now also intersects the lower stable manifold of W . This implies transport across the two halves of the cavity. A portion of fresh fluid which enters the cavity from one side is discharged into vortices on the opposite side. For example, Figure 11 shows how the fluid region from the upper stream marked E_{-1} is entrained into the cavity as E_o and then after one period is partly shed into both sides of the wake (see region E_1). The rate of transport of fluid across the upper and lower halves of the cavity can be quantified by considering the stable manifold of the middle surface point M in conjunction with the leftgoing unstable manifold of the wake point W . They are shown in Figure 13 for $Re = 100$ and $Re = 180$. The boundary of the two halves of the cavity may be defined as $MO''W$; it is shown using "railroad tracks" for $Re = 180$. The shaded regions depict

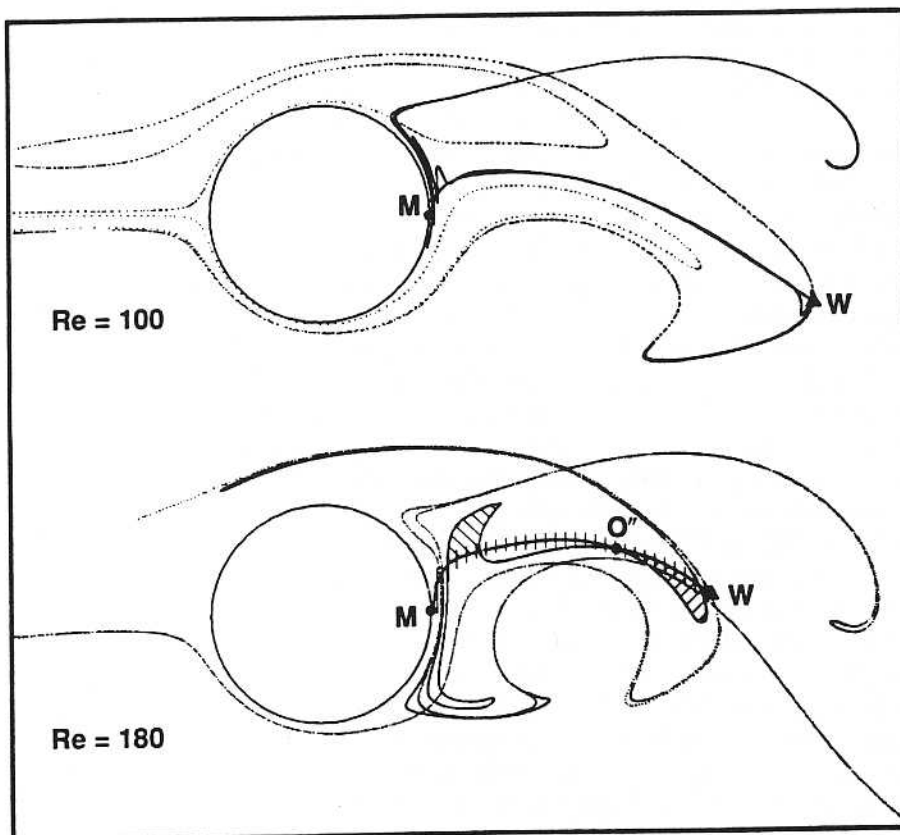


FIGURE 13. The leftgoing unstable manifold of W and the stable manifold of M are shown for two Reynolds numbers. They illustrate the degree of fluid transport across the upper and lower halves of the cavity.

successive iterates of fluid which is transported from the lower to the upper cavity. For $Re = 100$, the splitting of the two manifolds is confined to near the fixed points and a very small area of fluid (not shaded) is exchanged across the two halves.

Manifolds, streak visualization and vorticity. In earlier work (Shariff *et al.* [20], [21]) it was found for leapfrogging vortex rings that smoke injected across the entire diameter of the orifice by Yamada and Matsui [29] corresponded very well with the computed unstable manifold. The manifold could not penetrate the core of the vortices in the inviscid confined vorticity model which was employed, suggesting that had smoke been introduced as a streakline at the lip of the orifice where the vorticity was emitted, there would be little correspondence between manifold and smoke. Fortunately, the method of smoke injection of Yamada and Matsui placed smoke throughout the region of tangle of the manifolds where it gets drawn out along the unstable manifold. Similarly, for the present study our experience has been that the boundary of a rectangular patch placed in the wake cavity reveals more structure of the unstable manifold as time progresses.

However, in most experimental flow visualization for bluff bodies, tracer is injected continuously at fixed locations in space. These locations may be either on the surface of the body or upstream/downstream of the body. In the first category is Taneda [23] who employs electrostatic precipitation in water to generate a colloidal cloud on the entire surface of the body. The photograph on the cover of Van Dyke's [26] album was generated in this fashion. Taneda refers to the resulting object as an "integrated streaksheet." Gerrard [7] prepaints the surface with a strong solution of dye and then allows it to dry. Perry *et al.* [16] inject a ribbon of dye through a small porthole on the surface at 80° from the front stagnation point; by "ribbon" we mean that a tracer band of finite thickness is introduced. In the second category are Zdravkovich [32], who introduced a smoke ribbon at varying y levels upstream of the body, and Cimbala *et al.* [5] who employ a smoke wire to introduce streak ribbons at several y -locations simultaneously.

Let us note that because a streakline must emanate from a fixed location where the velocity cannot always be zero, while the manifold has no fixed location other than where the velocity is always zero, that their definitions never overlap. However, some streaklines can approximate the unstable manifold very well. For example, Figure 14 compares an unstable manifold with a simulated Taneda-Gerrard streaksheet. The streaksheet is drawn out along the manifold and further downstream differences between the two become imperceptible. Figure 15 compares a manifold with a streak-ribbon injected at 90° from the front stagnation point. This attempts to simulate the method of injection of Perry *et al.* [16]. One boundary of the ribbon agrees well with the manifold with a slight difference in regions of high curvature, while the other boundary has larger differences in regions of high curvature. It should clear from the preceding plot that for smoke wire injection far upstream of the cylinder, only the smoke released near $y = 0$ would agree with the manifold because it passes close to the surface. For injection further downstream, the largest y one could introduce tracer and still observe attraction to the manifold would be determined by the height of the E_i , ($i < 0$) lobes.

FIGURE 14
streaksheet
was obtained
at every time

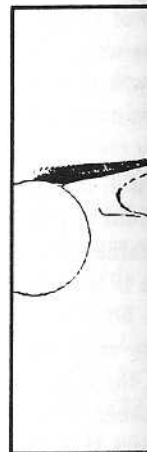


FIGURE 15
introduced
agrees well v

We often
tivity. Hama
in shear flow
of a streakli
the streamw
present in m
necessarily i
reason for th
pattern of st
degree the fl

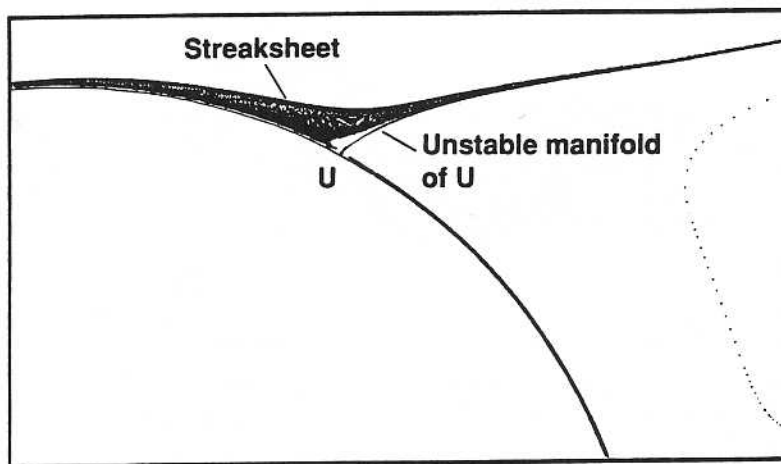


FIGURE 14. Unstable manifold of U compared with a Taneda-Gerrard streaksheet near the surface of the cylinder ($Re = 100$). The streaksheet was obtained by introducing particles all around the surface at $r = 1.004$ at every time step.

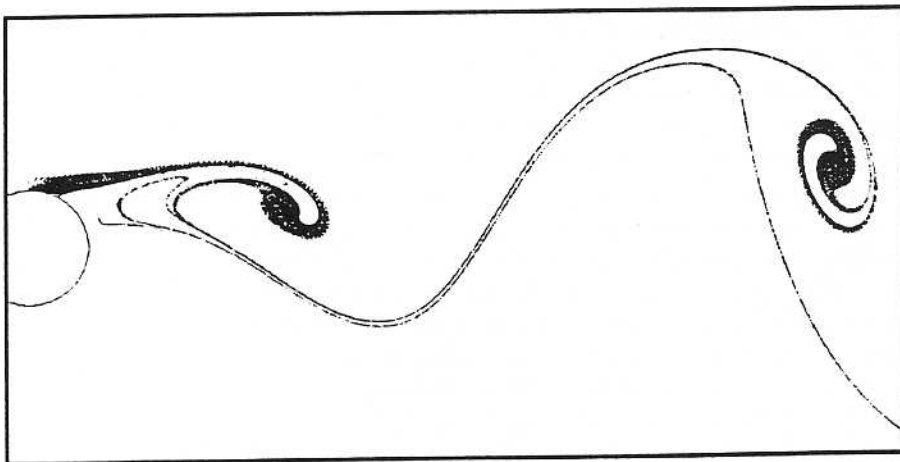


FIGURE 15. Unstable manifold of U compared with a streak-ribbon introduced at $\theta = 90^\circ$ ($Re = 100$). The inner boundary of the ribbon agrees well with the manifold.

We often rely on flow visualization to tell us something about the vorticity. Hama [9] cautioned that there are two features of flow visualization in shear flows which may lead to misinterpretation: (i) Lateral growth of a streakline can occur even when the vorticity is spatially periodic in the streamwise direction. Lateral streakline growth in the near wake is present in many published photographs of flow past a cylinder—it does not necessarily imply growth of any measure of hydrodynamic thickness. The reason for the growth is given by appealing to the uniformly propagating pattern of streamlines of the von Kármán model which represents to some degree the flow downstream of the body. A streakline injected in a region

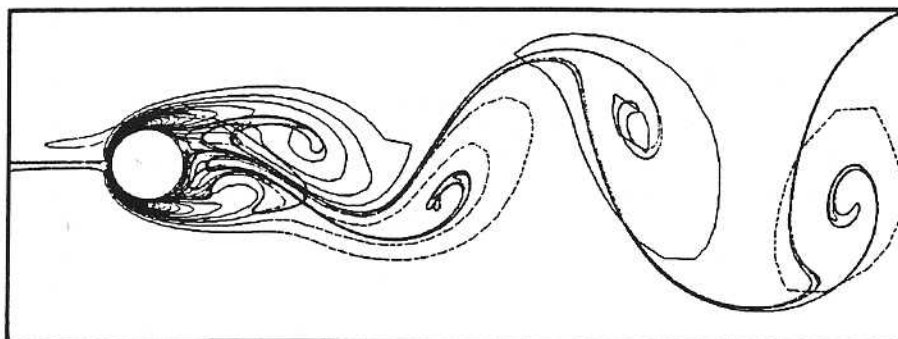


FIGURE 16. Manifolds compared with vorticity contours ($Re = 100$). The manifolds shown are: the unstable manifolds of U and L and the stable manifold of M .

of closed streamlines grows in lateral extent as each particle revolves on the closed streamline on which it was placed. (ii) For the steadily propagating model once again, centers of a streakline coil do not correspond to vorticity peaks except for a streakline injected at the appropriate y -level. Figure 16 compares vorticity contours with manifolds for $Re = 100$; the unstable manifolds can be considered to be a good representation of streaklines injected close to the cylinder. Points of zero curvature of the unstable manifold lie very close to vorticity peaks. There is lateral growth of the manifold as one travels downstream, but for the present Reynolds numbers it is matched by diffusion of vorticity.

Fluid in the vortex cores consists of only a small portion of fluid, in the form of tongues, shed from the cavity; most of it consists of fluid which acquired vorticity as it flowed over the body without being entrained into the cavity. The periodic point W has almost zero vorticity; this is true at other phases also. Except near the surface of the cylinder, the boundary of the two halves of the cavity also divides positive and negative vorticity and one may wonder whether transport across the two halves of the cavity for $Re = 180$ implies intrusion of vorticity of one sign into another. The feature labelled as A in the vorticity contours of Figure 17 shows that it does. It would be interesting to investigate the extent to which this process contributes to the annihilation of shed vorticity.

Manifolds and stretch. In this sub-section we consider the stretching of infinitesimal fluid elements as a means of rationalizing the close agreement between flow visualization and the unstable manifolds. Knowledge of the stretching of infinitesimal line elements is also important in problems such as drop break-up (Tjahadi and Ottino [24]) and molecular mixing (see Beige *et al.* [4] for a recent discussion relating stretch, molecular mixing and manifolds).

We ask: which infinitesimal line elements originating in the near wake stretch the most? Figure 18 shows the result after evolving a rectangular lattice of particles for two periods. From the deformation gradient matrix of each particle, the initial direction of the line element attached to it which maximizes the stretch, together with the value of the maximized

FIGURE 1. that the sl the upper 12.2].

stretch, we the rather are shown, at their in Elements v at the time initially ne (compare v manifolds secondary verified th points. If Ottino [22] periods en vortices, b way of dete the most is which line periods. O orientation those parti are now ne stretch wh

Minchin chin [15] of of a circula that partic nated upst

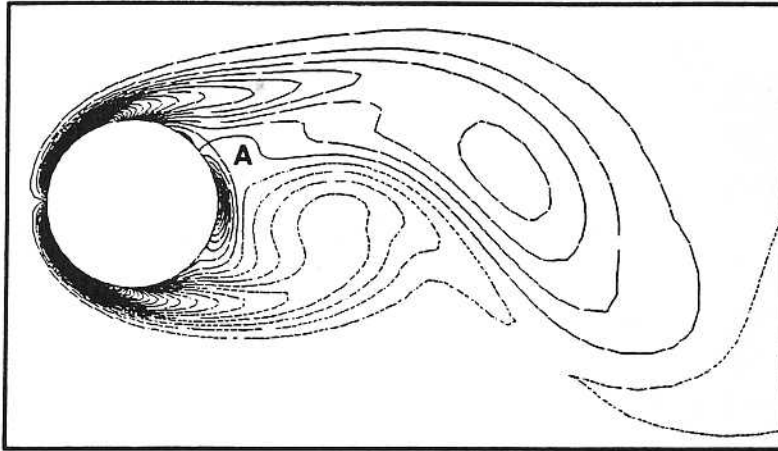


FIGURE 17. Vorticity contours for $Re = 180$. The feature 'A' indicates that the shaded fluid region in Figure 13 transports negative vorticity into the upper half of the cavity. Sixty levels are plotted in the range $[-14.25, 12.2]$.

stretch, were determined. Only particles with maximized stretch above the rather low threshold of 10% of the range above the minimum stretch are shown; therefore the stretching is very localized. Elements are plotted at their initial location with the initial maximizing direction indicated. Elements which have left the computational domain are assigned the values at the time of exit. One observes, with some exceptions, that line elements initially near and normal to the *stable* manifolds of W stretch the most (compare with Figure 8). With more periods, finer structure of the stable manifolds is revealed. Beige *et al.*[4] discuss the relevance of points of secondary intersection between the unstable and stable manifolds and we verified that some of the points which have the largest stretch are such points. If we plot particles at their *current* positions, as in Swanson and Ottino [22], we find that elements which have the largest stretch after two periods end up in the "braid" portions of the unstable manifolds between vortices, but so do other elements which do not stretch very much. A better way of determining which points in the current configuration have stretched the most is to run a rectangular lattice of particles backward in time and ask which line elements compress the most. Figure 19 shows the result for two periods. Only line elements having stretch factors (minimized over initial orientation) in the lowest 5% of the range are plotted. One concludes that those particles in the current configuration which have stretched the most are now near and parallel to the unstable manifold. Notice a reduction of stretch where the streak ribbon in Figure 15 clumps.

Minchin's [15] experiment. In §1 we mentioned the observation by Minchin [15] of the reversal of time-averaged temperature gradient downstream of a circular cylinder. It suggests, if heat conduction effects are neglected, that particles at some y -locations downstream must on average have originated upstream on the opposite side of the centerline. To test this, the code

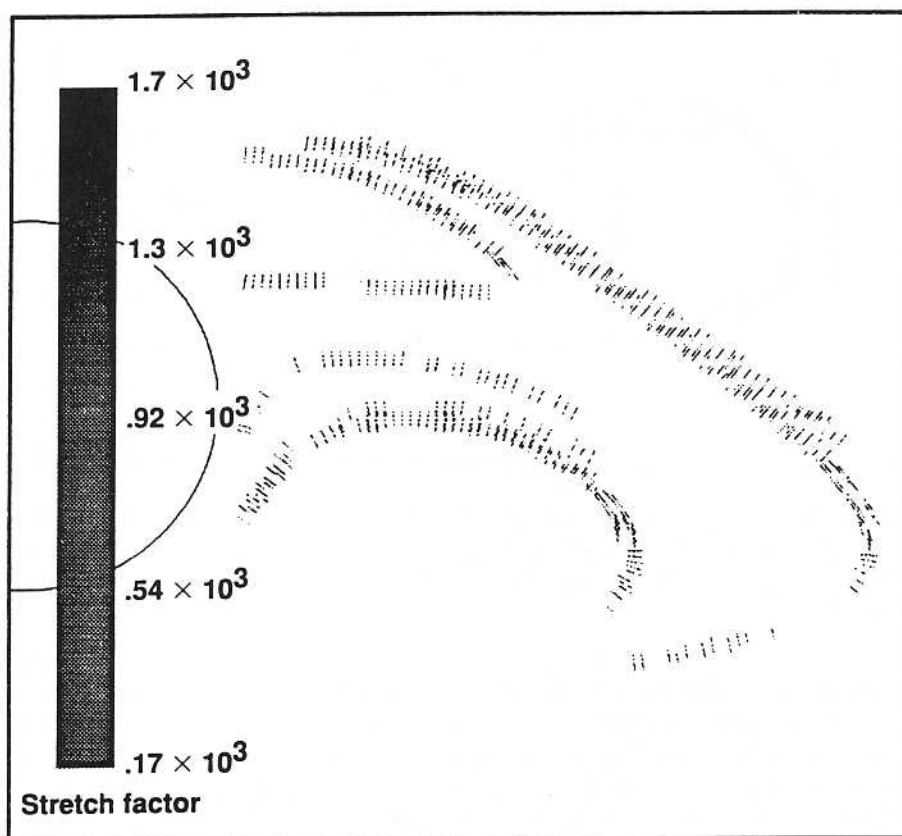


FIGURE 18. Initial positions and orientations of infinitesimal line elements which stretch the most after two periods ($Re = 100$). 100×100 elements were initialized on a rectangular lattice and only those having stretch (maximized over initial orientations) above a certain threshold, discussed in the text, are shown. An attempt is made to show the stretch factor of each element by gray-scaling.

was run backward in time and a vertical line of particles was introduced at a downstream location at every time step for the duration of one period. When particles crossed an upstream station, their y coordinates were recorded. Figure 20 plots each vertical line of particles, using as abscissa the time step at which it was introduced. Particles are colored by their y -location upstream; pure white indicates a particle which is trapped in the wake cavity and has not yet crossed the upstream station. One notices that at certain instants all the fluid exiting from $y \in [-4, 4]$ originated from a single side of the wake. This is what one would expect either from streakline photographs by noting that a streakline is a flexible barrier that separates fluid on the two sides of it, or from the smoke visualizations of Zdravkovich [32]. It is more difficult to anticipate the behavior of \bar{y} , the upstream value of y averaged for particles leaving downstream at $y = y'$ during a period.



FIGURE 20. Downstream y coordinate versus time step at which a vertical line of particles was introduced. The color of each line indicates the upstream y location. The color bar indicates the stretch factor.

FIGURE 21. Downstream y coordinate versus time step at which a vertical line of particles was introduced. The color of each line indicates the upstream y location. The color bar indicates the stretch factor.

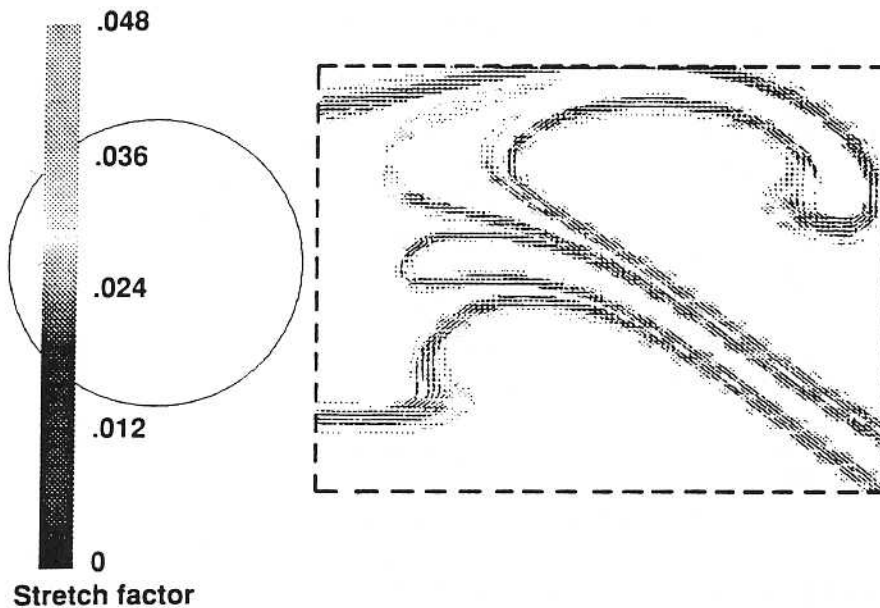


FIGURE 19. Infinitesimal line elements currently on a rectangular lattice (100×100) which have stretched the most in the last two periods. The gray-scale bar is for the inverse of the stretch since, as explained in the text, particles were run backward in time.

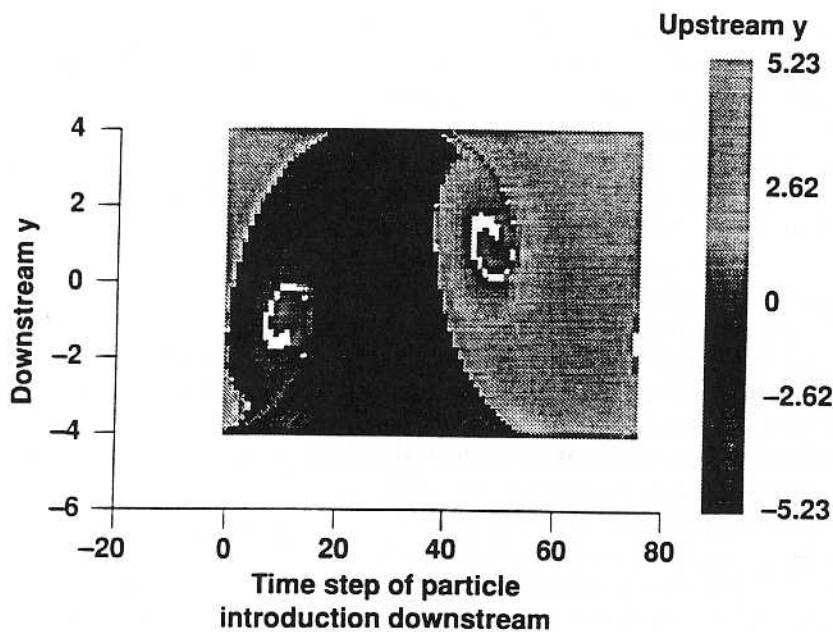


FIGURE 20. Vertical lines of particles introduced for one period at the downstream station $x = 18$ with time running backward. Each particle is shaded according to its y value at the upstream station $x = -2$.

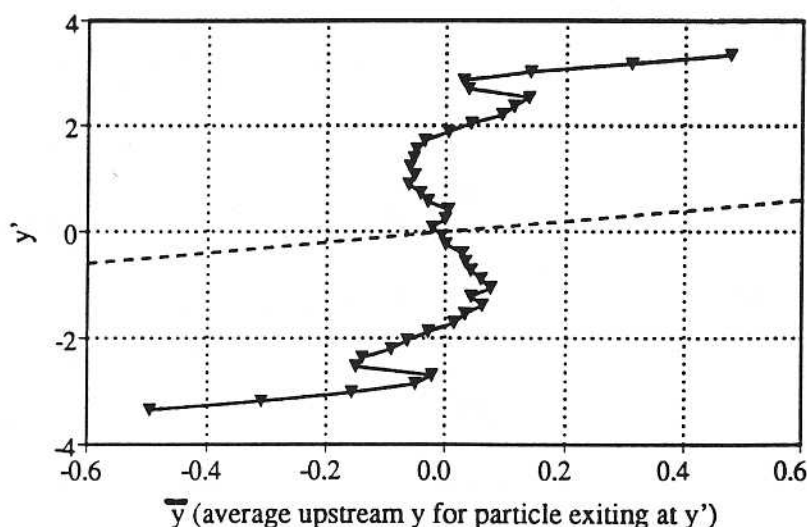


FIGURE 21. Average of the upstream y -value of particles exiting downstream during a period (solid triangles); ----, result if cylinder were absent.

The computed result is shown as the symbols in Figure 21 for $Re = 180$; trapped particles were not included in the average. The dashed line has a slope of unity and is the analog of the temperature profile upstream. The value of \bar{y} is practically uniform (in comparison with the dashed line) over a width of two cylinder diameters and the analog of temperature gradient reversal is present to a degree comparable to the sketch in Minchin [15]. For $Re = 100$, the region exhibiting uniform \bar{y} and the reversal effect were smaller. It is natural to want to make further inquiry about the extent to which transport of fluid across the two halves of the cavity enhances the reversal effect and the extent to which the von Kármán model of steadily translating vortices is also able to display it.

5. Recommendations.

At least for time-periodic flows, the unstable manifold appears to be a good tool for numerical flow visualization. It would be interesting to investigate whether manifolds defined for maps during some event in a non-periodic flow also share this property in some way. It may be asked why one is in need of a tool for numerical flow visualization in the first place—why not simply use many particles to simulate the tracer injection technique of the experiment? The answer is that it is difficult to place particles with enough resolution everywhere tracer is injected. The unstable manifold is an evolving curve for two-dimensions and the calculations suggest that it is a type of attractor. This means that (i) The dimensionality of the problem is reduced and it is easier to maintain resolution and (ii) A wide range of initial conditions will tend to reveal its structure as time progresses. These remarks must be tempered by the fact that to date the unstable manifold has been investigated for time-periodic or quasi-periodic (Beige *et al.*[3]) flows.

The last
physical e
phenomen

(28)

may receiv
For exampl
Eckert-We
cylinder in
temperatur
temperatur

(29a)

(29b)

Consider t
to the righ
 $f(\psi)$, on e
(29a) vanis

(30)

where u_x is
in (30) expl
is hotter or
terclockwis
the rear su
argument.

Open flow
chaotic par
entrained in
periods bef
transient ch
simple (ever
flow. Simila
For example
quadratic m
critical valu
region $x \in [$
to the cylind
the number
(more so nea
the residence
stirred cavit
circular cylin

The last part of the previous section, attempted to explain an interesting physical effect by means of a Lagrangian argument. We believe that many phenomena governed by an equation of the form

$$(28) \quad \frac{D\phi}{Dt} = \text{source term},$$

may receive insight by a study of the evolution of ϕ following fluid particles. For example, Kurosaka *et al.*[12] look to a Lagrangian explanation of the Eckert-Weise effect in which the wall temperature at the rear of a circular cylinder in compressible flow is colder than even the free-stream static temperature. The explanation uses the evolution equation of stagnation temperature (in the absence of viscosity and conduction):

$$(29a) \quad c_p \frac{DT_s}{Dt} = \frac{P_{,t}}{\rho},$$

$$(29b) \quad T_s \equiv \frac{T + |\mathbf{u}|^2}{2c_p}.$$

Consider the pattern of streamlines of the von Kármán model propagating to the right at uniform speed U_p . In the steady frame T_s is a constant, say $f(\psi)$, on each streamline, by virtue of the fact that the right hand side of (29a) vanishes. Therefore in the laboratory frame

$$(30) \quad T_s = f(\psi) + \frac{U_p^2}{2c_p} + \frac{u_x U_p}{c_p},$$

where u_x is the streamwise velocity in the moving frame. The last term in (30) explains why on a clockwise streamline the stagnation temperature is hotter on the top side than on the bottom and vice-versa for a counterclockwise streamline. However it does not, in our opinion, explain why the rear surface of the body is cold; this may require a truly Lagrangian argument.

Open flows such as the one we considered in this paper display *transiently* chaotic particle paths: a particle streaming towards the cylinder may be entrained into the cavity and display irregular motion for a finite number of periods before being shed into the wake. Many other systems also exhibit transient chaos and it may be worthwhile to study them or to concoct simple (even 1-D) maps which have the general behavior of the cylinder flow. Similarities and differences with the cylinder may prove illuminating. For example according to Grebogi, Ott and Yorke [34], the one-dimensional quadratic map exhibits a transition from chaos to transient chaos above a critical value of some parameter, whereby iterates gradually escape the region $x \in [-2, 2]$ and are swept to $x = -\infty$; this is somewhat analogous to the cylinder flow but the quadratic map is not one-to-one. The decay of the number of "particles" from the region $x \in [-2, 2]$ is nearly exponential (more so near the transition); this is unlike the cylinder flow. Furthermore, the residence time is predicted well by invoking the assumption of the well-stirred cavity. What are the essential reasons why the behavior of the circular cylinder flow defies such simple laws?

It is necessary for many applications involving wake flows to consider the behavior of particles which have inertia, drag, added-mass, etc. and there have been some attempts towards applying dynamical systems theory ideas to this problem. Since the velocity components of each particle enter as extra dimensions in the phase space a geometric approach similar to the one adopted here would not be the first method of attack. Rather at first, an investigation of the statistical properties of particle distributions seems to be preferred. For example, for a model closed flow, Yu, Grebogi and Ott [31] found that the system can exhibit behaviors typical of dissipative systems, for example, particles in physical space can concentrate on a fractal set, and in a recent talk, Wen *et al.*[35] have characterized particle distributions in wake flows in terms of the correlation dimension but a lot more work needs to be done before transport rates or particle collection rates at the surface can be predicted.

Acknowledgements

The authors are grateful to the Numerical Aerodynamic Simulation Program at NASA Ames Research Center for the provision of computer time. Dr. Philippe Spalart helped by suggesting that the point of zero time averaged shear stress would be the best place to numerically start looking for the manifold emanation point on the surface of the body. The analysis that this point is exactly the emanation point was inspired by the suggestion of Dr. D. Barkley and Prof. I. Kevrekides of Princeton Univ. that this point had to be independent of phase. It is a pleasure to recall that our interest in the problem began at another workshop on Vortex Methods in 1987 (at UCLA) when the editors of this volume spoke of the sketch in Perry *et al.*[16] depicting the winding back and forth of a streakline in the flow past a cylinder.

REFERENCES

1. R.H. Abraham and C.D. Shaw, *Dynamics—The Geometry of Behavior. Part 3: Global behavior*, Aerial Press, Inc., Santa Cruz, Calif., 1981.
2. G.K. Batchelor, *An Introduction to Fluid Dynamics*, Cambridge University Press: Cambridge, England, 1967.
3. D. Beige, A. Leonard and S. Wiggins, *Chaotic transport in the homoclinic and heteroclinic tangle regions of quasiperiodically forced two dimensional dynamical systems*, Nonlinearity (to appear).
4. D. Beige, A. Leonard and S. Wiggins, *A global study of enhanced stretching and diffusion in chaotic tangles*, Preprint.
5. J.M. Cimbalá, H.M. Nagib and A. Roshko, *Large structure in the far wakes of two-dimensional bluff bodies*, J. Fluid Mech. 190 (1988), 265–298.
6. B.E. Eaton, *Analysis of laminar vortex shedding behind a circular cylinder by computer-aided flow visualization*, J. Fluid Mech. 180 (1987), 117–145.
7. J.H. Gerrard, *The wakes of cylindrical bluff bodies at low Reynolds number*, Phil. Trans. Roy. Soc. Lond. A 288 (1978), 351–382.

8. J. C. Bifurcation
9. F.R. in the
10. W. the
11. G.E. in the
12. M. H. K. 178
13. Sir R. Rosen
14. A.S. of the
15. L.T. tution
16. A.E. men
17. T.H. conv 0360
18. V. R. Phys
19. V. R. mizi
20. K. S. of co
21. K. S. NAS
22. P.D. study
23. S. Ta. Sci. 1
24. M. T. J. Fl
25. C.H. tion of the & C.
26. M. V.
27. J.H. Engin
28. G. W. Symp 1265
29. H. Ya. vorte
30. P.K. simu
31. L. Yu. of pa H.C.
32. M.M. street

8. J. Guckenheimer and P. Holmes, *Nonlinear Oscillations, Dynamical Systems, and Bifurcations of Vector Fields*, Springer Verlag: New-York, Heidelberg, Berlin, 1983.
9. F.R. Hama, *Streaklines in a perturbed shear flow*, *Phys. Fluids* **5** (1962), 644-50.
10. W. Humphries and J.H. Vincent, *Experiments to investigate transport processes in the near wakes of disks in turbulent air flow*, *J. Fluid Mech.* **75** (1976), 737-749.
11. G.E. Karniadakis and G.S. Triantafyllou, *Frequency selection and asymptotic states in laminar wakes*, *J. Fluid Mech.* **199** (1989), 441-469.
12. M. Kurosaka, J.B. Gertz, J.E. Graham, J.R. Goodman, P. Sundaram, W.C. Riner, H. Kuroda and W.L. Hankey, *Energy separation in a vortex street*, *J. Fluid Mech.* **178** (1987), 1-29.
13. Sir M.J. Lighthill, *Boundary layer theory*, in "Laminar Boundary Layers (ed. L. Rosenhead)," Dover, 1963.
14. A.S.M. MacLennan and J.H. Vincent, *Transport in the near aerodynamic wakes of flat plates*, *J. Fluid Mech.* **120** (1982), 185-197.
15. L.T. Minchin, in "Proceedings of the General Discussion on Heat Transfer," Institution of Mechanical Engineers, London, 1951, p. 45.
16. A.E. Perry, M.S. Chong, and T.T. Lim, *The vortex-shedding process behind two-dimensional bluff bodies*, *J. Fluid Mech.* **116** (1982), 77-90.
17. T.H. Pulliam and J.L. Steger, *Recent improvements in efficiency, accuracy, and convergence for implicit approximate Factorization Algorithms*, AIAA Paper 85-0360, AIAA 23rd Aerospace Sciences Meeting, Reno, Nev., Jan. 1985.
18. V. Rom-Kedar, *Transport rates of a class of two-dimensional maps and flows*, *Physica D* **43** (1990), 229-268.
19. V. Rom-Kedar, A. Leonard, and S. Wiggins, *An analytical study of transport, mixing and chaos in an unsteady vortical flow*, *J. Fluid Mech.* **214** (1990), 347-394.
20. K. Shariff, A. Leonard, N.J. Zabusky and J.H. Ferziger, *Acoustics and dynamics of coaxial interacting vortex rings*, *Fluid Dyn. Res.* **3** (1988), 337-343.
21. K. Shariff, A. Leonard, and J.H. Ferziger, *Dynamics of a class of vortex rings*, NASA TM 102257, 1989.
22. P.D. Swanson and J.M. Ottino, *A comparative computational and experimental study of chaotic mixing of viscous fluids*, *J. Fluid Mech.* **213** (1990), 227-249.
23. S. Taneda, *Visual study of unsteady separated flows around bodies*, *Prog. Aerospace Sci.* **17** (1977), 287-348.
24. M. Tjahjadi and J.M. Ottino, *Stretching and breakup of droplets in chaotic flows*, *J. Fluid Mech.* (to appear).
25. C.H.K. Williamson, *2-D and 3-D aspects of the wake of a cylinder, and their relation to wake computations*, in "Vortex dynamics and vortex methods (Proceedings of the AMS-SIAM Conference) Lectures in Applied Mathematics (ed. C. Anderson & C. Greengard)," Amer. Math. Soc., Providence, R.I., 1990, pp. ???-???
26. M. Van Dyke, *An Album of Fluid Motion*, Parabolic Press, Stanford, Calif., 1982.
27. J.H. Vincent, *Particle dynamics in a grid-type electrostatic precipitator*, *Chem. Engin. Sci.* **32** (1977), 1077-1082.
28. G. Winterfeld, *On processes of turbulent exchange behind flame holders*, in "Tenth Symposium on Combustion," The Combustion Institute, Pittsburgh, 1965, pp. 1265-1275.
29. H. Yamada and T. Matsui, *Preliminary study of mutual slip-through of a pair of vortex rings*, *Phys. Fluids* **22** (1978), 292-294.
30. P.K. Yeung and S.B. Pope, *An algorithm for tracking fluid particles in numerical simulations of homogeneous turbulence*, *J. Comp. Phys.* **79** (1989), 373-416.
31. L. Yu, C. Grebogi and E. Ott, *Fractal structure in physical space in the dispersal of particles in fluids*, in "Nonlinear Structure in Physical Systems (ed. L. Lam and H.C. Morris)," Springer-Verlag, New York, 1990, pp. 223-231.
32. M.M. Zdravkovich, *Smoke observations of the formation of the a Kármán vortex street*, *J. Fluid Mech.* **37** (1969), 491-496.

33. E.E. Zukoski and F.E. Marble, *Experiments concerning the mechanism of flame blowoff from bluff bodies*, in "Proceedings of the Biennial Gas Dynamics Symposium on Aerothermochemistry (1955) (ed. D.K. Fleming)," Northwestern Univ., 1956, pp. 205-210.
34. C. Grebogi, E. Ott and J.A. Yorke, *Crises, sudden changes in chaotic attractors and transient*, Physica D 7 (1983), 181-200.
35. F. Wen, L. Tang, Y. Yang, C.T. Crowe, J.N. Chung and T.R. Troutt, Bull. Am. Phys. Soc. 35 (1990), 2297.

K.S. & T.H.P.:

NASA AMES RESEARCH CENTER, MOFFETT FIELD, CALIF. 94035

E-mail address: SHARIFF@WK64.NAS.NASA.GOV

J.M.O.:

UNIVERSITY OF MASSACHUSETTS, AMHERST, MASS. 01003